

This work was written as part of one of the author's official duties as an Employee of the United States Government and is therefore a work of the United States Government. In accordance with 17 U.S.C. 105, no copyright protection is available for such works under U.S. Law.

Public Domain Mark 1.0

<https://creativecommons.org/publicdomain/mark/1.0/>

Access to this work was provided by the University of Maryland, Baltimore County (UMBC) ScholarWorks@UMBC digital repository on the Maryland Shared Open Access (MD-SOAR) platform.

Please provide feedback

Please support the ScholarWorks@UMBC repository by emailing scholarworks-group@umbc.edu and telling us what having access to this work means to you and why it's important to you. Thank you.

Global Soil Water Estimates as Landslide Predictor: The Effectiveness of SMOS, SMAP, and GRACE Observations, Land Surface Simulations, and Data Assimilation

ANNE FELSBERG,^a GABRIËLLE J. M. DE LANNOY,^a MANUELA GIROTTI,^b JEAN POESEN,^{a,c}
ROLF H. REICHLÉ,^d AND THOMAS STANLEY,^{e,f,g}

^a Department of Earth and Environmental Sciences, KU Leuven, Heverlee, Belgium

^b Department of Environmental Sciences Policy and Management, University of California, Berkeley, Berkeley, California

^c Faculty of Earth Sciences and Spatial Management, Maria Curia-Skłodowska University, Lublin, Poland

^d Global Modeling and Assimilation Office, NASA Goddard Space Flight Center, Greenbelt, Maryland

^e Universities Space Research Association, Columbia, Maryland

^f Goddard Earth Sciences Technology and Research, Columbia, Maryland

^g Hydrological Sciences Laboratory, NASA Goddard Space Flight Center, Greenbelt, Maryland

(Manuscript received 25 September 2020, in final form 5 February 2021)

ABSTRACT: This global feasibility study assesses the potential of coarse-scale, gridded soil water estimates for the probabilistic modeling of hydrologically triggered landslides, using Soil Moisture Ocean Salinity (SMOS), Soil Moisture Active Passive (SMAP), and Gravity Recovery and Climate Experiment (GRACE) remote sensing data; Catchment Land Surface Model (CLSM) simulations; and six data products based on the assimilation of SMOS, SMAP, and/or GRACE observations into CLSM. SMOS or SMAP observations (~40-km resolution) are only available for less than 20% of the globally reported landslide events, because they are intermittent and uncertain in regions with complex terrain. GRACE terrestrial water storage estimates include 75% of the reported landslides but have coarse spatial and temporal resolutions (monthly, ~300 km). CLSM soil water simulations have the added advantage of complete spatial and temporal coverage, and are found to be able to distinguish between “stable slope” (no landslide) conditions and landslide-inducing conditions in a probabilistic way. Assimilating SMOS and/or GRACE data increases the landslide probability estimates based on soil water percentiles for the reported landslides, relative to model-only estimates at 36-km resolution for the period 2011–16, unless the CLSM model-only soil water content is already high (≥ 50 th percentile). The SMAP Level 4 data assimilation product (at 9-km resolution, period 2015–19) more generally updates the soil water conditions toward higher landslide probabilities for the reported landslides, but is similar to model-only estimates for the majority of landslides where SMAP data cannot easily be converted to soil moisture owing to complex terrain.

KEYWORDS: Hydrology; Hydrometeorology; Soil moisture; Satellite observations; Data assimilation; Land surface model

1. Introduction

Landslides are downslope mass movements that can lead to significant economic or infrastructural damages and fatalities (Petley 2012; Froude and Petley 2018). They occur sporadically in space and time (Froude and Petley 2018), depending on environmental, climatic, or geophysical conditions (Whiteley et al. 2019). The most prominent spatial preconditioning factors are the local topography and geology (Reichenbach et al. 2018); landslides occur most frequently in areas with steep local relief and with hillslope materials of low shear strength. Time-variant preconditioning factors can be of anthropogenic, seismic, or hydrometeorological (climatic or seasonal) nature. In this study, we focus on the latter, taking into account solely hydrologically triggered landslides.

To prevent loss of life and mitigate damages, efforts are made to predict the likelihood of landslides by determining and monitoring the conditions leading to landslides (hereafter

referred to as “landslide modeling”). Slope stability or failure is a result of two opposing forces: the shear strength and shear stress. When shear stress exceeds shear strength, the slope fails. This can result from (i) decreases in the strength and/or (ii) increases in the stress. Increased soil water content can have both these effects, through (i) decreasing the friction at the shear plane and (ii) increasing the weight of the soil (Whiteley et al. 2019), as illustrated in Fig. 1. Physically based landslide models calculate the ratio between shear stress and strength, often referred to as “factor of safety” (Whiteley et al. 2019). Since this requires detailed information about the slope in question, the approach is computationally intensive and limited to small-scale applications.

For larger or data-scarce areas, empirical models have been developed to predict the likelihood of landslide occurrence. Often, these empirical models use rainfall thresholds as indicators for the moisture state of the soil (Guzzetti et al. 2007). Most of these thresholds have been created for well-documented, landslide-prone areas, but Caine (1980) and Hong et al. (2006) derived global rainfall intensity–duration thresholds, and recent studies used national high-resolution rainfall data from a gauge network (Leonarduzzi et al. 2017) or satellite products (Rossi et al. 2017). Alternatively, thresholds have been determined based on antecedent rainfall. Such weighted, cumulative sums of rainfall

Denotes content that is immediately available upon publication as open access.

Corresponding author: Anne Felsberg, anne.felsberg@kuleuven.be

DOI: 10.1175/JHM-D-20-0228.1

© 2021 American Meteorological Society. For information regarding reuse of this content and general copyright information, consult the AMS Copyright Policy (www.ametsoc.org/PUBSReuseLicenses).

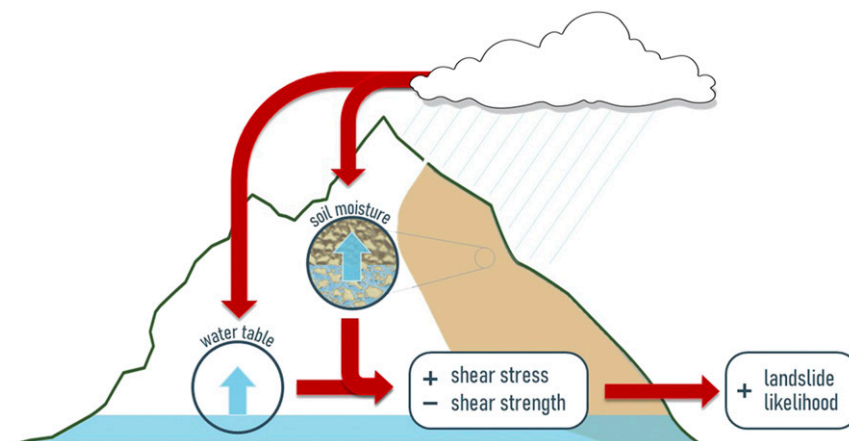


FIG. 1. Schematic of hydrological processes leading to the initiation of a landslide.

mimic the water content of the soil and have been used for regional to global landslide modeling (Glade et al. 2000; Monsieus et al. 2019; Kirschbaum and Stanley 2018).

However, empirical landslide models based solely on precipitation products have large numbers of false-positive predictions because they lack information on predisposing soil hydrologic conditions. Combining thresholds on rainfall and soil moisture (trigger and cause) can significantly decrease this number of false alarms (Bogaard and Greco 2018), regardless of the soil moisture data source. Mirus et al. (2018) found reduced false-positive prediction for a combination of 15-day antecedent in situ soil saturation and 3-day cumulative rainfall for two sites in Washington and Oregon, United States. For two regional landslide early warning systems in Italy, the inclusion of simulated soil moisture obtained from two different models (Segoni et al. 2018; Ponziani et al. 2012) improved the predictions' reliability and robustness. Rescaling of simulated soil moisture toward in situ and satellite observations (Brocca et al. 2016) added to this effect. For one of these Italian regions, Zhuo et al. (2019) developed satellite-based slope-dependent soil moisture thresholds. When using satellite products, Brocca et al. (2016), Kirschbaum et al. (2020), Thomas et al. (2019), and Zhuo et al. (2019) recommend the use of satellite-derived data products of soil moisture in deeper layers (at least 1 m) rather than satellite retrievals of surface (0–5 cm) soil moisture conditions, because the shear planes of both deep-seated and shallow landslides are typically much deeper than 5 cm. Estimates of the deeper soil moisture based on physically based land surface models were preferred (Brocca et al. 2016; Kirschbaum et al. 2020; Thomas et al. 2019) and found to be superior compared to those of, for example, simple exponential filters (Zhuo et al. 2019).

Apart from their use in conjunction with thresholds, satellite-derived soil moisture and rainfall were also successfully used in a multilinear regression to predict tension crack openings at a study site in Italy (Brocca et al. 2012), and in multivariate machine learning toward a landslide hazard indicator for Oregon and Washington (Stanley et al. 2020). In situ soil moisture metrics were moreover successfully combined in a logistic regression to predict landslide probability in Switzerland (Wicki et al. 2020).

While spatially distributed soil moisture data are already being used in landslide modeling at the local to regional and soon global scale, the potential of various remotely sensed and simulated estimates of soil moisture and water storage has not yet been evaluated globally for landslide modeling. This study aims at investigating to which extent global landslide modeling can benefit from various global data products. One option are remote sensing data. Here, we will investigate the potential of two L-band (1.4 GHz) microwave satellite missions that are dedicated to soil moisture monitoring, i.e., the Soil Moisture Ocean Salinity (SMOS) and Soil Moisture Active Passive (SMAP) missions (Kerr et al. 2012; Entekhabi et al. 2010). We further use data from the Gravity Recovery and Climate Experiment (GRACE) mission, which provides anomalies in the vertically integrated terrestrial water storage (TWS), including groundwater, soil moisture, snow, surface water, and water stored in the vegetation canopy (Swenson et al. 2003). See appendix B for a list of abbreviations used throughout this paper.

Satellite information is limited in space and time and to a small set of observable variables. Compared to satellite retrievals, soil water estimates obtained from land model simulations have fewer limitations in terms of spatiotemporal coverage or resolution. Models such as the Catchment Land Surface Model (CLSM; Koster et al. 2000) also provide estimates of soil moisture and the groundwater table at the typical depths of shallow landslide shear planes. In this paper, CLSM simulations of spatially and temporally complete coverage will be used to identify the probability of landslide occurrences as function of several land surface variables, beyond the traditional predictor variables of surface soil moisture or rainfall.

On the other hand, land surface models are prone to errors (e.g., due to missed precipitation events and uncertainties in model parameters). By combining CLSM simulations with SMOS, SMAP, and/or GRACE observations via data assimilation (DA), we can infer more accurate estimates of deeper soil moisture and groundwater table depths from surface observations (SMOS, SMAP; De Lannoy and Reichle 2016b; Reichle et al. 2017b) and vertically integrated TWS observations (GRACE; Zaitchik et al. 2008; Grotto et al. 2016). Such improvements in soil water estimates have the potential to

improve landslide modeling. In this paper, five SMOS and GRACE data assimilation experiments, and the operational SMAP Level-4 surface and root-zone soil moisture product (SMAP L4) will be evaluated for landslide occurrences. SMAP L4 was earlier used for landslide predictions near San Francisco Bay (Thomas et al. 2019), where the benefit of SMAP L4 could not be shown, because, on top of limitations in capturing detailed hillslope drainage processes, the coarse-scale satellite footprints over this heterogeneous region are dominated by urban and open water contamination and the data are possibly not assimilated. The SMAP L4 product is slated to be incorporated into Landslide Hazard Assessment for Situational Awareness (Kirschbaum et al. 2020).

Even though passive microwave and gravimetric satellite data, as well as global model simulations, have a spatial resolution that is too coarse to represent dynamic drainage processes or to estimate the location of a landslide on a hillslope, they do capture the overall temporal variations in water availability across the area and thereby have the potential to estimate the likelihood of a landslide occurrence in time. In practice, the latency in the availability of satellite data (ranging from days for SMOS or SMAP, to months for GRACE) could be bridged by using the latest available data to initialize (via data assimilation) model forecasts of land surface conditions. In the following, the term “landslide modeling” always refers to the relative probabilistic likelihood estimation in time (only), unless specified otherwise. To include the spatial dimension in the probabilistic likelihood estimation in future research, spatial susceptibility information could be used.

The objective of this paper is to address the following three questions: 1) Can remotely sensed observations of soil moisture from SMOS and SMAP or TWS from GRACE be of use for global landslide modeling? 2) Do simulations of soil water conditions by CLSM show a clear difference between “stable slope” and “landslide” conditions, and how do these soil water estimates discern slope conditions compared to state-of-the-art rainfall indices? 3) To what extent is data assimilation of SMOS, GRACE, or SMAP beneficial for global landslide modeling?

2. Data, model, and methods

a. Landslides

The term “landslide” in this study refers to all types of mass movements triggered by rainfall. The location, date, size, and trigger of a large number of landslides are taken from the Global Landslide Catalog (GLC; Kirschbaum et al. 2010, 2015) and from quarterly reports issued by the Russian Federation (FSBIH 2018). For the GLC, (hydrologically triggered) landslide occurrences are collected systematically based on media reports from 2007 onward. Our use of the Russian data mitigates the bias toward English-language reports in the GLC. However, an underrepresentation of landslide occurrences in many areas, such as South America and Africa, remains. The Russian data are limited to the period from 2010 to 2018.

Landslides where information on location or timing is unknown are excluded. We additionally exclude landslides of a

duration longer than 1 day (Russian data) and assume that GLC landslide occurrence dates imply a relatively short duration, which limits our analysis to fast-moving landslides. Of the hydrologically triggered landslides only those with the following GLC qualifiers are used: “continuous rain,” “downpour,” “monsoon,” “flooding,” “rain,” and “tropical cyclone,” and for the Russian data, “rainfall” and “unknown.”

For comparison with gridded remote sensing and model data, multiple landslides on the same day within one grid box of the corresponding spatial resolution are aggregated into one landslide event (LSE) and their size and trigger attributes are randomly selected from the collection of contributing landslides. Unless noted otherwise, for the remainder of the paper the term landslide refers to a (hydrologically triggered) landslide event that occurred on one day and in one grid box as defined above.

b. Soil moisture and water storage estimates

1) SATELLITE DATA

The study period in this paper is constrained by the availability of landslide data and satellite observations from GRACE and L-band microwave missions, as illustrated in Fig. 2. Because of the complementarity of SMOS and GRACE and their relatively long period of overlap, this paper will focus on SMOS and GRACE from 1 January 2011 through 31 July 2016 (hereafter referred to as the SMOS-GRACE study period). We separately investigate SMAP data from 1 April 2015 through 31 December 2019 (hereafter referred to as the SMAP study period).

Since 2010, the SMOS mission has been observing L-band brightness temperature T_b with a revisit time of 2–3 days and a spatial resolution of about 40 km. This study uses the Level 1 (L1) and Level 2 (L2) SMOS products, separately. The L1 T_b observations at horizontal (H) and vertical (V) polarization were extracted from the SCLF1C v620 product, fitted to a 40° incidence angle, mapped onto the 36-km Equal-Area Scalable Earth version 2 (EASEv2) grid, quality controlled as in De Lannoy and Reichle (2016a) and Bechtold et al. (2019), and are referred to as SMOS- T_b hereafter. The L2 soil moisture retrievals of the SMUDP2 v650 product were processed to the 36-km EASEv2 grid as in De Lannoy and Reichle (2016b). These soil moisture retrievals pertain to the 5-cm-thick top layer, hereafter referred to as “surface,” as marked in Fig. 3. The retrievals are accompanied with quality flags that allow the user to apply a more or less conservative data screening. For minimum quality data (SMOS-SM0), mountain ranges, ice, and glaciers as well as areas with radio frequency interference (RFI) are excluded. For higher-quality data (SMOS-SM1), areas with dense forests, near open water, with dense population, or any other concern raised in the science flags are additionally excluded. These options cover some common approaches to quality flagging in literature, and the results will show that constraining data to SMOS-SM1 quality standards reduces data availability at landslide occurrences by one order of magnitude.

Similar to SMOS, the SMAP mission observes L-band T_b at H and V polarization, albeit at a fixed 40° incidence angle and

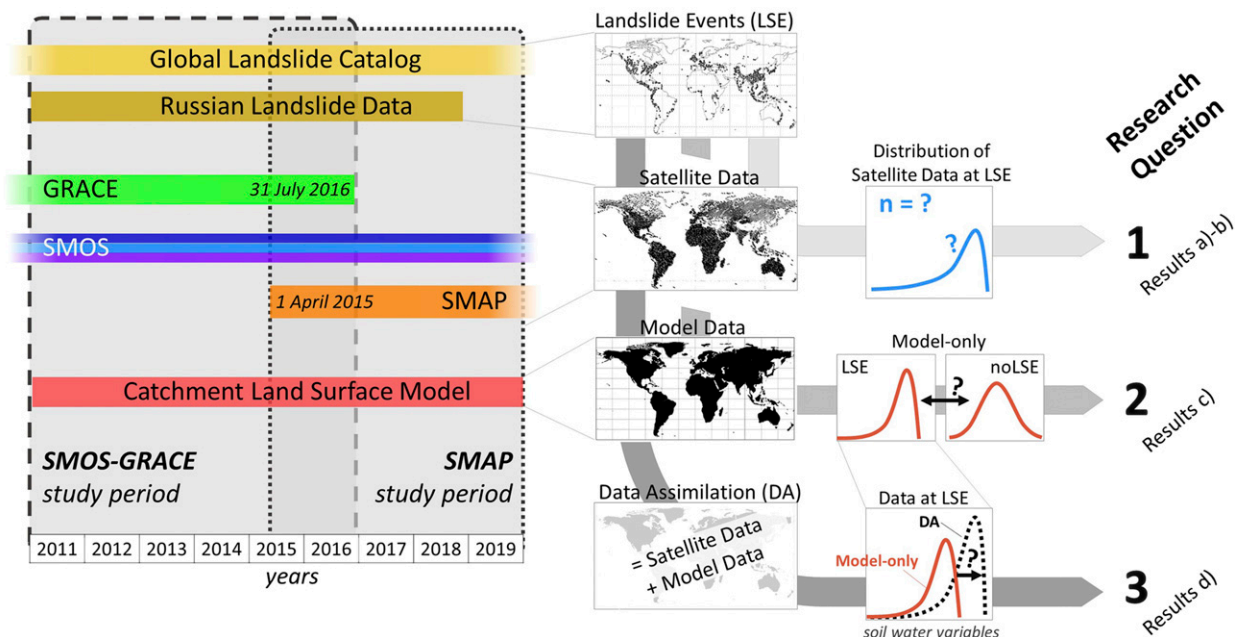


FIG. 2. Schematic of this study, with overview of datasets used, definition of the two study periods, usage of data for each research question, and subsection that includes the corresponding results.

with improved RFI mitigation compared to SMOS (Piepmeier et al. 2017) leading to soil moisture retrievals that are often superior to those from SMOS (Chen et al. 2018). This study will focus on soil moisture estimates from the SMAP L4 product (version 4) (Reichle 2018; Reichle et al. 2019) which is based on the assimilation of L1C (version 4) T_b observations, hereafter referred to as SMAP- T_b .

The GRACE mission observed Earth's time-varying gravity field (Swenson et al. 2003) from March 2002 until 31 July 2016. Temporal deviations in gravity from the seasonal average are attributed to changes in TWS across the entire soil column (see Fig. 3). We use mass concentration block (mascon) solutions produced by the Goddard Space Flight Center (GSFC; (Luthcke et al. 2013; Loomis et al. 2019). These provide monthly averaged TWS observations with a spatial resolution of approximately 300 km. We use the standard solutions with the ICE-6G model glacial isostatic adjustment (Peltier et al. 2015).

2) CATCHMENT LAND SURFACE MODEL

CLSM is a state-of-the-art, physically based land surface model (Koster et al. 2000) that can be run offline (land-only) or coupled with the atmosphere in the Goddard Earth Observing System (GEOS) modeling framework. As illustrated in Fig. 3, CLSM provides estimates of surface (0–5 cm, sfmc), root-zone (0–100 cm, rzmc), and profile (from 0 cm to bedrock, prmc) soil moisture. These moisture variables are diagnosed from the so-called catchment deficit (catdef) model prognostic variable, which measures the amount of water that would be needed to bring the catchment to saturation and is proportional to the water table depth, and from two additional (surface and root-zone) water excess variables, srfezc and rzexc, that simulate deviations from the equilibrium soil moisture profiles. CLSM

was chosen for this study because it is one of only a few available global land surface models that dynamically simulate shallow water table depths, and because CLSM is also used in the generation of the SMAP L4 product (Reichle et al. 2019).

In this study, all CLSM simulations are performed offline, after a multidecade spinup. The land surface parameters, including the information on soil texture (De Lannoy et al. 2014), match those of the operational SMAP L4 product. Note again that this study only focuses on the relative temporal variations in land surface variables, which are only secondarily affected by, e.g., soil and vegetation parameters. These parameters would primarily determine the spatial (static) distribution of landslide susceptibility. For the SMOS-GRACE study period, the

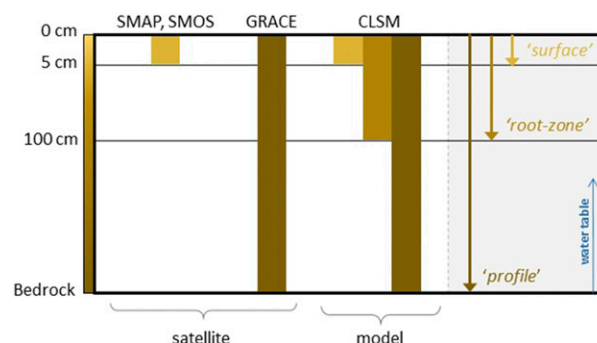


FIG. 3. Overview of different observed and simulated soil water content stores. SMOS and SMAP observe T_b sensitive to conditions within the upper 5 cm of the soil. GRACE observes anomalies of TWS, which includes soil moisture and groundwater. CLSM models all TWS components except for surface water.

spatial resolution is 36 km and meteorological forcing data were extracted from the Modern-Era Retrospective Analysis for Research and Applications, version 2 (MERRA-2; [Gelaro et al. 2017](#)), without precipitation corrections, as in [De Lannoy and Reichle \(2016b\)](#) and [Giroto et al. \(2016, 2019\)](#). For the SMAP study period, we use CLSM as configured in version 4 of the SMAP L4 ([Reichle et al. 2019](#)) with a spatial resolution of 9 km and surface meteorological forcing data from the GEOS Forward Processing (FP) with gauge-based precipitation corrections. Although gauge-based corrected precipitation also exists for MERRA-2, the rain gauge densities in mountainous remote areas tend to be rather low ([Kidd et al. 2017](#)) and we opted not to use the correction. For each study period, one model-only (open loop, OL) simulation is performed, i.e., one at 36 km for the SMOS-GRACE study period and one at 9-km resolution for the SMAP study period. All OL simulations and data assimilation results presented in this study are ensemble averages of 24 members, obtained by slightly perturbing select forcing and state variables to account for model uncertainties, following [Giroto et al. \(2019\)](#). If not mentioned otherwise, “model” within this paper always refers to CLSM.

3) DATA ASSIMILATION

Data assimilation (DA) integrates satellite observations into model simulations, while accounting for uncertainties in each data source. By assimilating microwave-based data related to sfmc, and/or gravity-based TWS retrievals, it is possible to update water content estimates in all layers of the soil profile. DA further allows dynamic downscaling and interpolation of coarse-scale observations. At the same time, the observations help to correct the model for missing processes or errors in meteorological forcings. For example, precipitation estimates obtained from global circulation models may poorly represent convective rain events ([Dai 2006](#)), which are crucial for landslide modeling.

In this paper we present results of six different DA systems. For the SMOS-GRACE study period, five 36-km systems assimilate either SMOS or GRACE data separately or together. For the SMAP study period, the 9-km operational SMAP L4 product is used. All systems use a spatially distributed ensemble Kalman filter, but their updated state variables differ slightly, depending on the assimilated observations. Details are summarized in [Table 1](#).

The assimilation of GRACE TWS (DA_GRACE) follows the procedure detailed in [Giroto et al. \(2016\)](#), the assimilation of SMOS-Tb, SMOS-SM0, or SMOS-SM1 soil moisture retrievals (DA_SMOS-Tb, DA_SMOS-SM0, DA_SMOS-SM1) follow [De Lannoy and Reichle \(2016b\)](#), and the joint assimilation of GRACE TWS and SMOS-SM0 (DA_SMOS-GRACE) follows [Giroto et al. \(2019\)](#), but with the difference that here GSFC mascon solutions are used ([Luthcke et al. 2013](#); [Loomis et al. 2019](#)). The SMAP L4 product ([Reichle et al. 2019](#)) is referred to as DA_SMAP-Tb for consistency with the other experiment names, and its finer spatial resolution might represent local landslide conditions better. Also note that SMAP T_b data offer better coverage than the SMOS T_b after quality control.

In all DA experiments, bias between the satellite observations and model simulations is removed, so that OL, observation, and

TABLE 1. Overview of the two model-only (open loop, OL) and six data assimilation (DA) experiments used in this study. DA experiments are grouped per study period (SMOS-GRACE, SMAP). For each case, we list the assimilated satellite data, the updated CLSM soil water variables, references, and information on the perturbations, the forcing data, spatial resolution, and other details. Note that all experiments from the SMOS-GRACE study period also use the CLSM system from the operational SMAP L4 product.

Experiment	Assimilated data		Updated soil water variables		Reference	Perturbations, forcings, other details	
	Model-only (OL)	DA_GRACE	None	GRACE TWS	None	catdef	
SMOS-GRACE	DA_SMOS-SM0	SMOS-SM0	sfmc, rzmc		Giroto et al. (2016) , but using GSFC mascon solutions (Luthcke et al. 2013 ; Loomis et al. 2019) De Lannoy and Reichle (2016b)	sfmc, rzmc sfmc, rzmc sfmc, rzmc sfmc, rzmc, catdef	Perturbations of Giroto et al. (2019) and MERRA-2 forcings without precipitation corrections, on EASEv2 grid (36 km).
	DA_SMOS-SM1	SMOS-SM1	sfmc, rzmc				
	DA_SMOS-Tb	SMOS-Tb	sfmc, rzmc				
	DA_SMOS-GRACE	GRACE TWS and SMOS-SM0	sfmc, rzmc, catdef				
SMAP	Model-only (OL)	None	None		Reichle et al. (2019)	sfmc, rzmc	Perturbations of Reichle et al. (2017b) and GEOS FP forcings with gauge-based precipitation correction, on EASEv2 grid (9 km).
	DA_SMAP-Tb (identical to SMAP L4)	SMAP-Tb	sfmc, rzmc				

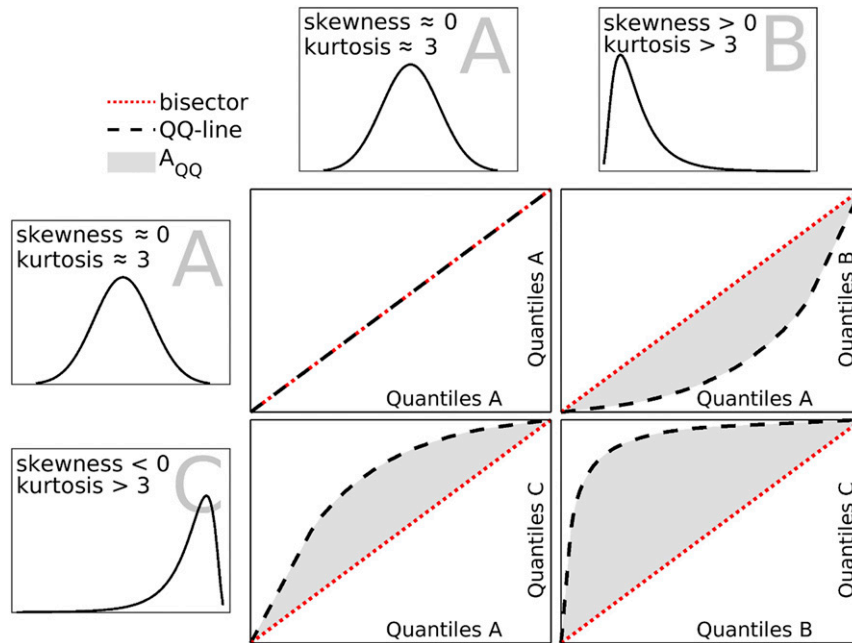


FIG. 4. Example distributions and comparison metrics applied to them: skewness and kurtosis per distribution (A–B–C), as well as QQ plots for combinations thereof.

DA climatologies are similar by design. The SMOS-Tb and SMAP-Tb are seasonally rescaled to the model climatology, whereas for SMOS-SM0 and SMOS-SM1, the bias correction involves cumulative distribution matching, and the GRACE TWS are rescaled to match the long-term mean and variance of the model simulations. The latter two bias correction approaches do not correct for seasonal phase shifts between assimilated observations and simulations, which might cause the resulting DA climatology to differ from that of the OL. Furthermore, the spatial filtering and nonlinear effects between variables might change the local climatology of DA results compared to that of the OL.

Earlier research (De Lannoy and Reichle 2016b; Giroto et al. 2016, 2019; Reichle et al. 2019; Qiu et al. 2021) confirmed the benefit of the above DA experiments using a multitude of in situ data in various regions of the globe. In situ measurements of landslide sites are limited to a small number of sites (e.g., Mirus et al. 2018, 2019; Thomas et al. 2019; Wicki et al. 2020). Due to this lack of sufficient in situ soil moisture and water table depth observations at the landslide sites investigated in this study, we cannot evaluate the DA estimates at all of our study locations. Our evaluation will instead indirectly assess the benefit of DA for the application of landslide probability calculations [section 2c(4)].

c. Evaluation

1) SOIL WATER CONTENT DISTRIBUTIONS

LSEs are sporadic in space and time, preventing a deterministic modeling or evaluation at the global scale. Instead, a stochastic approach is needed, whereby the probability of an

LSE, $p(\text{LSE})$, is estimated. This total probability can be broken up into different conditional probability parts $p(\text{LSE}|x_i)$, with x_i being various stochastic predictor variables, including static land features and time-variant variables. Even though a number of time-variant variables x_i contribute to the probability of an LSE, this paper only focuses on predictors related to soil water content variables and rainfall or their transformations.

Consider, for instance, $p(\text{LSE}|\text{rzmc})$, the probability distribution of an LSE conditioned on rzmc. Through Bayes's law, this conditional probability is directly related to $p(\text{rzmc}|\text{LSE})$, the probability distribution of rzmc conditioned on an LSE:

$$p(\text{LSE}|\text{rzmc}) = p(\text{rzmc}|\text{LSE}) p(\text{LSE}) / p(\text{rzmc}), \quad (1)$$

given a prior estimate of a landslide occurrence $p(\text{LSE})$, e.g., based on an area's landslide susceptibility, and the probability $p(\text{rzmc})$ of the occurrence of a particular rzmc value. The key distribution of interest in this paper is therefore $p(\text{rzmc}|\text{LSE})$ because it allows us to compute the desired probability of an LSE conditioned on rzmc, that is, $p(\text{LSE}|\text{rzmc})$.

2) PREDICTOR VARIABLES AND TRANSFORMATIONS

Besides $x_i = \text{rzmc}$, we sample $p(x_i|\text{LSE})$ for $x_i = \text{sfc}$, $x_i = \text{prmc}$ (related to soil moisture) and $x_i = \text{catdef}$ (related to the depth of groundwater table) by extracting satellite observations or daily CLSM simulations on the days and at the locations of observed LSE. Since catdef is inversely proportional to the total soil water content, we will invert catdef in the presentation of the results, so that the deepest water tables correspond to the driest conditions. Note that catdef output is

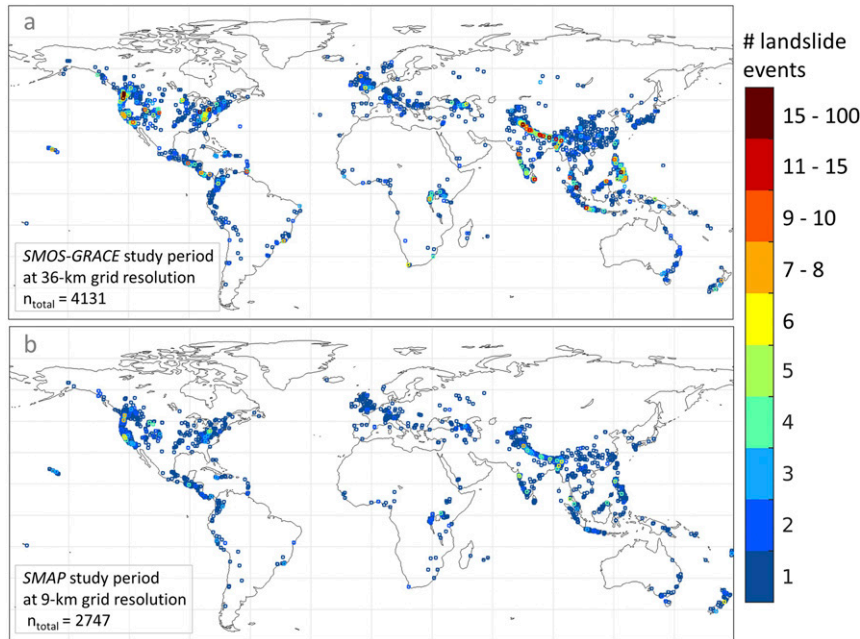


FIG. 5. Global distribution of hydrologically triggered landslide events (LSE) on the EASEv2 grid (each observed box is represented by a square). The number of LSEs per grid box is shown for the (a) SMOS-GRACE and (b) SMAP study period.

not published as part of the SMAP L4 operational data product and therefore only analyzed for the SMOS-GRACE study period. In addition, we analyze rainfall (CLSM input, i.e., from MERRA-2 and GEOS FP) and the 7-day antecedent rainfall index (ARI7), allowing comparison with other studies that use antecedent precipitation to mimic soil moisture (Kirschbaum and Stanley 2018). ARI7 is calculated for each day t as the weighted average w_t of antecedent rainfall r_t during the preceding 7 days:

$$\text{ARI7} = \frac{\sum_{t=0}^6 r_t w_t}{\sum_{t=0}^6 w_t}, \quad \text{where } w_t = (t+1)^{-2}. \quad (2)$$

The explaining variables x_i are further evaluated after transformations of the raw explanatory variables into percentiles, linearly rescaled values, and anomalies. Besides making data of different environmental conditions comparable, these transformations also inform about the extremity of certain conditions and might enable a stronger distinction between landslide and stable slope conditions. Both the transformations into percentiles and rescaling ensure a quasi-monotonous increase of $p(x_i|\text{LSE})$ with increasing x_i .

The percentiles $[1, \dots, 99]$ are defined relative to their long-term distribution. This is in line with using percentiles of antecedent precipitation for global landslide nowcasting (Kirschbaum and Stanley 2018). The linearly rescaled values were computed using the temporal maximum and minimum values within each grid box j , e.g., for rzmc , and span the interval $[0, 1]$:

$$\text{rzmc}_{j,\text{rescaled}} = \frac{\text{rzmc}_j - \min(\text{rzmc}_j)}{\max(\text{rzmc}_j) - \min(\text{rzmc}_j)}. \quad (3)$$

The anomaly time series are computed for each grid box as the short-term and interannual deviations from a multiyear, seasonally varying climatology obtained after first smoothing x_i with a 31-day moving window.

3) COMPARING DISTRIBUTIONS

Given the limitations of satellite observations alone in terms of observable variables and spatiotemporal coverage, we turn to CLSM simulations (OL) to identify the differences between the distributions of the various land surface variables x_i related to soil water content on days of LSE and on days with no landslide event (noLSE), i.e., $p(x_i|\text{LSE})$ and $p(x_i|\text{noLSE})$.

The LSE samples in our study are a (regionally biased, cataloged) subset of all possible landslide events. However, since we only focus on the temporal dependencies between water contents and landslide probabilities, our results may be applicable to unsampled areas, provided a universal validity of the underlying physics of hydrologically driven landslides.

The noLSE set includes all days without a landslide, excluding 3 days before and after a landslide record to account for inaccuracies in landslide event dating. It moreover includes only grid boxes with at least one observed landslide event during the study period. Grid boxes without any observed landslides are excluded, to avoid information from areas which are not prone to landslides or with undocumented landslides. The noLSE distribution does not change noticeably when the 3 days before and after the landslide are included (statistically equivalent, not shown), i.e., the noLSE

essentially covers the full time series of land surface variables at all grid boxes with a landslide. Our analysis only aims at identifying LSEs in a climatological sense and will not be able to distinguish between stable and potentially unstable conditions during, for example, a storm event. In the future, an analysis of the difference between LSEs and a strongly constrained set of noLSE occurrences within a season, or even within a storm, would add useful insight.

Differences between the LSE and noLSE distributions, i.e., the sampled $p(x_i|LSE)$ and $p(x_i|noLSE)$, are visualized through box plots and histograms and quantified by three measures, illustrated in Fig. 4: the area between the quantile–quantile (QQ) line and the bisector (A_{QQ}), the skewness (third moment of the distribution), and the kurtosis (fourth moment of the distribution). The QQ plot visualizes the shifts between two distributions by plotting values of the same quantile against each other. The closer this QQ line is located to the bisector, i.e., the smaller A_{QQ} , the more similar the two distributions are. We normalize A_{QQ} by the total area underlying the bisector in order to make A_{QQ} comparable between variables of different magnitudes. If a distribution is not perfectly normally distributed, the skewness indicates the side of the tail, and the kurtosis is a measure of how strongly the distribution is tailed compared to a normal distribution.

Even though the noLSE and LSE sample sizes are very different ($n_{noLSE} \approx 1100n_{LSE}$), both are large (>1000) enough to extract significant differences in statistical features that allow to set apart the LSE distribution in a long-term climatological sense.

4) ESTIMATING THE IMPACT OF DATA ASSIMILATION

The impact of DA on the estimation of landslide probabilities as a function of soil water estimates is assessed in terms of shifts in the probability distributions between OL and DA results when conditioned on days and locations of observed landslide events (LSE subset). As mentioned above, the time series of the OL and DA results have similar climatologies, but with some local differences. Additionally, the soil water estimates from OL and DA typically differ on any given single day as observations are assimilated in the DA experiments, and because of an accumulation of changes during the previous days to months. Consequently, when conditioned on LSE, the distributions of the OL and DA results are expected to differ.

Assuming soil water content to be proportional to landslide probability, it can be expected that the soil is most likely wet for observed landslide events, and if the DA results are reliable, then the analysis soil water contents should most likely be high. Consequently, we expect the DA to preferentially correct the model simulations toward wetter conditions, e.g., to correct for missed or underestimated rainfall events in MERRA-2 and GEOS FP, for unmodeled groundwater processes, etc. Of course, it is also possible that the DA leaves the soil water content unchanged, or reduces the moisture content, especially at times when the soil is already near complete soil saturation and no water can be added.

To quantify the DA impact on $p(rzmc|LSE)$, we determine the sign of the $rzmc$ differences between the DA and OL, at LSE:

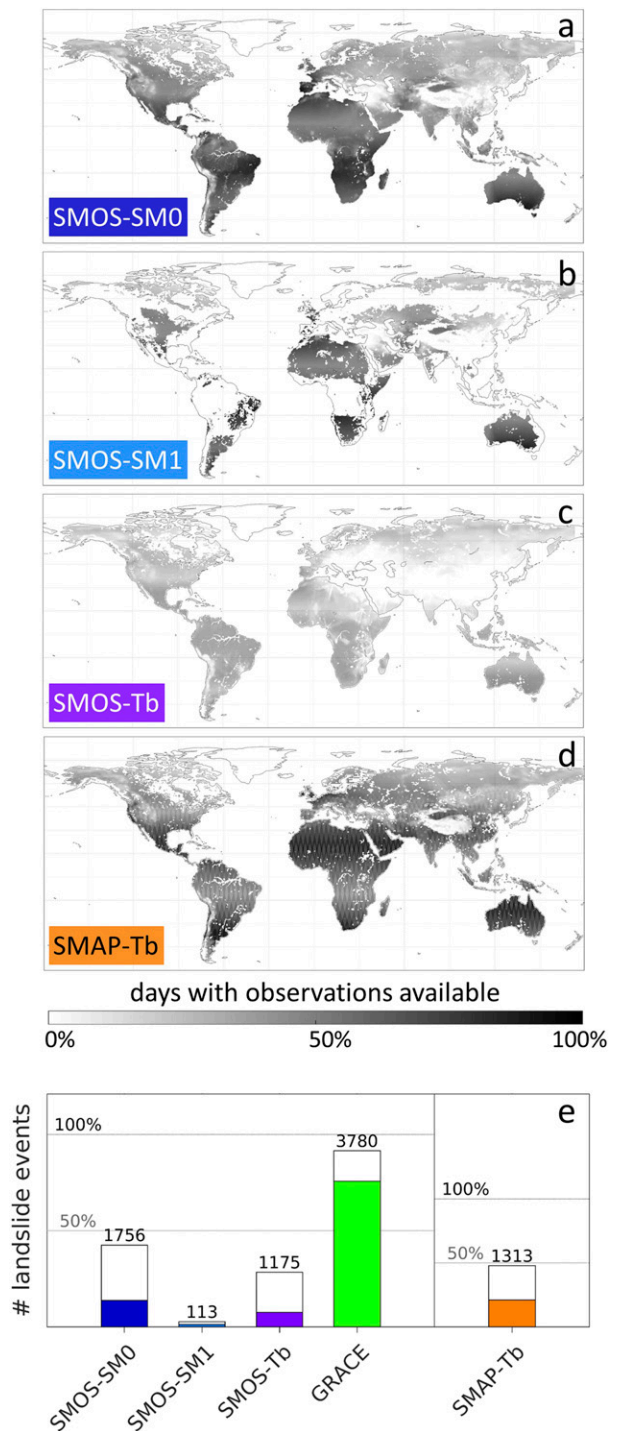


FIG. 6. Coverage of satellite observations in percent of observed days relative to the total number of days of the according study period, with (a)–(c) SMOS-SM0, SMOS-SM1, and SMOS-Tb counted during the SMOS-GRACE study period and (d) SMAP-Tb counted during the SMAP study period. (e) Number of landslide events that coincide with SMOS-SM0, SMOS-SM1, SMOS-Tb, GRACE TWS, and SMAP-Tb observations. In color: counted only when observations exist on the exact day of the landslide event; white: additional coverage when taking into account prior observations, either during the last week (SMOS, SMAP) or month (GRACE) before the event. Numbers indicate the sum of both.

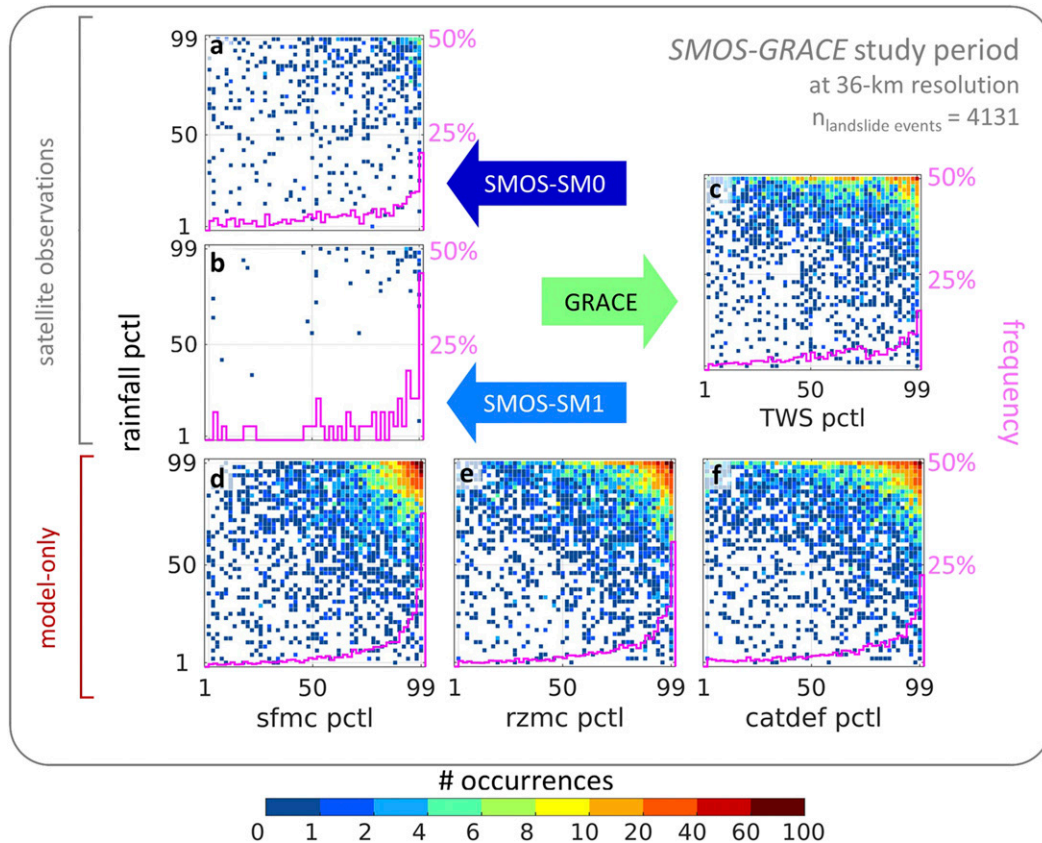


FIG. 7. Joint distribution of daily soil water content and MERRA-2 rainfall conditioned on the occurrence of landslide events [$p(x_i|\text{LSE})$] during the SMOS-GRACE study period, for (a)–(c) observed SMOS SM0 or SM1 or GRACE TWS and (d)–(f) simulated CLSM model-only (OL) water content variables: (left) sfmc, (center) rzmc, (right) catdef. The values are transformed into percentiles (pctl) within each 36-km grid box. The pink lines show the marginal conditional distributions of daily soil water content variables conditioned by LSE. Reference noLSE distributions are uniform (horizontal lines; not shown). The total number of LSEs in each subpanel is determined by the availability of simulated (all LSE) or observational (subset of LSE) data, see Fig. 6e.

$$\Delta \text{rzmc} = \text{rzmc}_{\text{DA}} - \text{rzmc}_{\text{OL}}, \quad (4)$$

and count the number of positive and negative Δrzmc (i.e., rzmc increases $\Delta \text{rzmc}, +$ and decreases $\Delta \text{rzmc}, -$) that exceed a minimum absolute threshold of 2% of the maximum rzmc_{OL} value per grid box. We hypothesize that, at observed landslides, the number of increases ($n_{\Delta \text{rzmc}, +}$) would be larger than that of decreases ($n_{\Delta \text{rzmc}, -}$). The rzmc is chosen as predictor variable, because it is directly updated by all SMOS, SMAP and GRACE DA experiments (Table 1), and it is sensitive to both surface soil water content and groundwater information. We count $n_{\Delta \text{rzmc}, +}$ and $n_{\Delta \text{rzmc}, -}$ for volumetric rzmc values ($\text{m}^3 \text{m}^{-3}$) and after transformation into linearly rescaled values [Eq. (3)], percentiles and anomalies [section 2c(3)]. Since the latter two transformations are computed relative to the respective (not completely identical) climatologies of OL and DA rzmc, the signs of Δrzmc might change for different transformations, altering $n_{\Delta \text{rzmc}, +}$ and $n_{\Delta \text{rzmc}, -}$.

Counts are summarized per DA experiment for all landslide events (LSE subset), as well as additionally stratified by pre-conditioning local or temporal characteristics:

- for grid boxes with at least one satellite observation in the study period;
- for days with OL rzmc < 50th percentile;
- for landslides triggered by a “downpour” (i.e., convective rainfall event), for shallow and deep landslides (see appendix A).

Another approach would be to analyze the cumulative DA analysis increments in the month preceding a landslide. We have verified that this approach leads to similar findings, but the specific nature of DA increments renders them more complex to give guidelines for landslide modeling.

3. Results

a. Landslide events and satellite data

Figure 5 shows the spatial distribution of landslide occurrences for the SMOS-GRACE and SMAP study periods at the EASEv2 grid 36- and 9-km resolution, respectively. Landslides typically occur in mountainous regions or in coastal areas with steep and high cliffs, and with either strong seasonal rain events

such as the Asian Monsoon, or a high frequency of shorter rainfall events as in Ireland or Great Britain. A total of 4735 landslides, aggregated to 4131 landslide events at 36-km resolution, occur during the SMOS-GRACE study period, and a total of 2903 landslides, aggregated to 2747 landslide events at 9-km resolution, occur during the SMAP study period.

Based on these landslide events, we aim to answer our first research question whether remotely sensed soil moisture or TWS data alone can be of use for landslide modeling. Figures 6a–d show how the SMOS and SMAP coverage varies for the various data products and quality flagging. The SMOS-Tb data are strictly limited here to the alias-free zone within the full swath, while the SMOS-SM0 and SMOS-SM1 retrievals are retained in the extended alias-free zone (De Lannoy and Reichle 2016b), explaining the lower percentage of SMOS-Tb data compared to that of SMOS-SM0. Comparing Figs. 6a–d and 5 reveals that the areas with the highest landslide density (mountain ranges, such as the Himalayas) happen to have the lowest numbers of useful SMOS and SMAP observations (SMOS-SM0, SMOS-Tb, SMAP-Tb) or nearly none at all (SMOS-SM1). Complex terrain complicates the radiative transfer processes and hence the interpretation of T_b data as well as the retrieval of soil moisture. In addition, an important region in Asia suffers from RFI.

The colored bars in Fig. 6e show that useful SMOS observations are available on the day of a landslide event for 571 (or 13.8%) for SMOS-SM0, 55 (or 1.3%) for SMOS-SM1 and 313 (or 7.6%) for SMOS-Tb of the 4131 landslides during the SMOS-GRACE study period. When assuming that SMOS observations up to 7 days before the landslide would still be informative at the day of the event (as is done for some other applications, Koster et al. 2019), the numbers increase. But despite this temporal gap filling, there are still only useful data available for less than 50% of landslide events: 1756 (or 42.5%) for SMOS-SM0, 113 (or 2.7%) for SMOS-SM1, and 1175 (or 28.4%) for SMOS-Tb. SMAP-Tb observations are available for 582 (or 21.2%) of the 2747 landslide events during the SMAP study period at the day of the event and 1313 (or 47.8%) when considering observations within 7 days. Despite having global coverage, GRACE TWS data are only available for 3129 (or 75.7%) of the landslides at the day of the event and 3780 (or 91.5%) when propagating observations into the following month. The GRACE observation gaps are caused by satellite battery management issues. These numbers underline that SMOS, SMAP, or GRACE data alone are not suitable for global landslide modeling.

b. Observed and simulated soil water content distributions at landslide events

Despite their limitations, the available satellite retrievals on the days and at locations of landslide events (LSE, no propagation in time) still provide useful insights into the joint conditional probability distributions of the observed sfmc, TWS, as well as rainfall percentiles, shown in Figs. 7a–c: SMOS-SM0, SMOS-SM1 sfmc, and GRACE TWS all exhibit an exponential increase in probability for increasing water content and rainfall percentiles at LSE, but the increase in TWS is not as strong as for sfmc. Keep in mind that SMOS-SM1 is a subset of SMOS-SM0 and only includes 55 LSE. The reference noLSE percentile distributions are by design uniform, because percentiles are

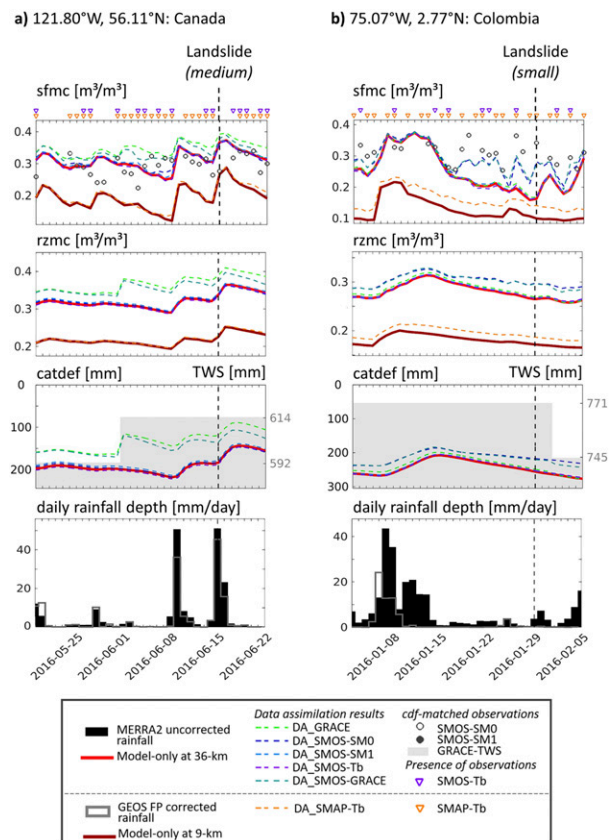


FIG. 8. Time series of model-only (OL) and DA land surface variables, along with (an indication of) satellite observations within two grid boxes with a landslide occurrence in (a) Canada (on 15 Jun 2016) and (b) Columbia (on 29 Jan 2016), marked by the vertical black dashed line. (top) OL and DA sfmc (lines), and observations of SMOS-SM0 and SMOS-SM1 (symbols) and indications of SMOS-Tb and SMAP-Tb (symbols at top); (top middle) OL and DA rzmc; (bottom middle) OL and DA catdef (left y axis, flipped) and GRACE TWS (gray area and right y axis); (bottom) daily sum of rainfall depth from (black) MERRA-2 or (gray) GEOS-5 FP with precipitation corrections. OL and DA results are shown at the 36- and 9-km resolution.

computed relative to the complete time series at landslide locations, which is practically identical to the noLSE time series.

Figures 7d–f show the bivariate conditional probability distributions of CLSM OL sfmc, rzmc, catdef, and rainfall for LSE. These distributions are similar to those for the satellite observations, but more robust, because modeled data are available for all landslide events. Again, there is a steady increase in probability for higher water content and rainfall percentiles for LSE. This holds for both study periods, and thus both at 36- and 9-km resolution and both with uncorrected and corrected rainfall forcing (only 36-km OL results are shown). When combined with a high rainfall percentile (upper area of the bivariate density plot), a wide range of percentile values for deeper soil water contents (rzmc, catdef) can lead to a landslide, whereas high percentile values for sfmc are needed. This can in part be attributed to the fact that the distributions show daily soil water content values and rainfall depths of the same day, i.e., the

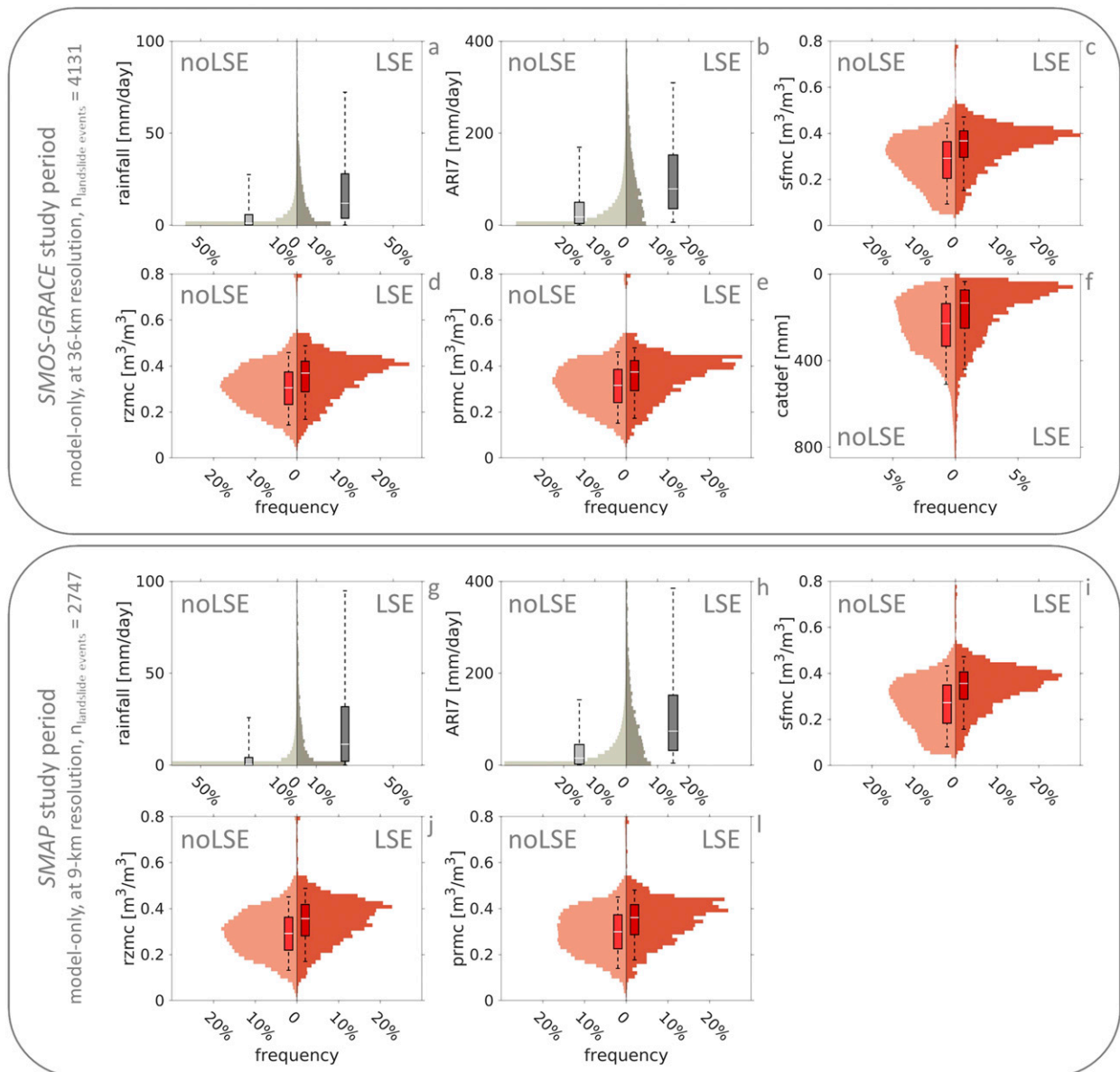


FIG. 9. Distribution of model-only (OL) land surface and rainfall variables (right, dark color) LSE and (left, light color) noLSE, shown in (background) histograms and (foreground) boxplots: (a),(g) daily rainfall (CLSM input), (b),(h) ARI7, (c),(i) daily sfmc, (d),(j) daily rzmc, (e),(l) daily prmc, and (f) daily catdef (note inverted axis). (top) SMOS-GRACE study period at 36-km resolution with uncorrected MERRA-2 rainfall; (bottom) SMAP study period at 9-km resolution with corrected GEOS-5 FP rainfall.

sfmc is a direct result of the rainfall. Deeper layers are less coupled to the surface, which explains why very low soil water contents in deeper soil layers more often coincide with high rainfall at LSE.

c. Comparing simulated soil water content distributions at landslide events and stable conditions

To address the question whether (and which) land surface model variables are able to distinguish between stable and potentially unstable slope conditions, we first present illustrative time series of three land surface variables at two locations where landslides occurred, and then evaluate whether the

spatiotemporal distributions of select land surface variables at LSE differ from their corresponding distributions at all other days (noLSE).

1) TIME SERIES

Figure 8 shows a 1-month time series of OL and DA sfmc, rzmc, and catdef, along with the rainfall forcing, leading up to and beyond a landslide event on 15 June 2016 in Canada (56.11°N, 121.80°W, Fig. 8a) and another landslide event on 29 January 2016 in Colombia (2.77°N, 75.07°W, Fig. 8b), for which observations of all three satellite products were

TABLE 2. Metrics comparing model-only (OL) LSE and noLSE distributions (as shown in Fig. 9), for rainfall, ARI7, sfmc, rzmc, prmc, and inverted catdef. Results are shown for the two study periods (SMOS-GRACE, SMAP) and without transformation of the variables. The CLSM output variable catdef was not recorded for the operational SMAP L4 product or its corresponding OL.

	36-km OL (SMOS-GRACE study period)					9-km OL (SMAP study period)				
	A_{QQ}	Skewness		Kurtosis		A_{QQ}	Skewness		Kurtosis	
		LSE	noLSE	LSE	noLSE		LSE	noLSE	LSE	noLSE
Rainfall	0.59	3.05	5.76	18.48	56.84	0.71	3.53	14.97	23.13	1138.70
ARI7	0.47	1.71	3.54	6.92	21.44	0.61	2.37	6.80	10.38	157.84
sfmc	0.20	-0.42	0.17	4.55	3.57	0.24	-0.29	0.25	4.26	3.42
rzmc	0.12	-0.12	0.50	4.13	4.65	0.15	-0.06	0.51	3.92	4.49
prmc	0.11	-0.16	0.42	4.32	4.48	0.13	-0.07	0.46	4.16	4.35
catdef	0.22	-1.60	-1.08	6.62	4.97	—	—	—	—	—

available and an effect of data assimilation is clearly visible. The 36- and 9-km results have different absolute values, mainly because of differences in their soil and vegetation parameters and rainfall input shown in the bottom panels of Figs. 8a,b). For this section, we only focus on the OL results (red lines). Both 36- and 9-km OL sfmc and rzmc respond fast to rainfall, whereas catdef reacts much more slowly and is dampened.

The landslide in Canada (Fig. 8a), noted to be of medium size (volume between 10 and 1000 m³) and triggered by a downpour, occurred on the day of a rainfall peak with a preceding rainfall event of similar magnitude one week earlier. Sfmc, rzmc, and catdef all indicate wet conditions in both the 36- and 9-km simulations. Overall, 1460 landslides during the SMOS-GRACE study period (703 during the SMAP study period) coincided with a peak of rainfall (exceeding the local median rainfall) and for another 1346 (688) landslides a rainfall peak occurred within the preceding week. However, the absence of rainfall peaks for nearly half of the 4131 (2747) landslide events indicates that landslide events also occur during moderate rain events of longer duration, or in the presence of other water sources (e.g., snowmelt). Another possibility is that the rainfall peak was missed in the MERRA-2 or GEOS FP data, or that the date of the landslide event was erroneous.

An example of a landslide in the absence of a rainfall peak is shown in Fig. 8b. The landslide in Colombia, noted to be small (volume < 10 m³), occurs after a longer period of rainfall but with only little or no rainfall on the day of slope failure for MERRA-2 or GEOS FP, respectively. Consequently, the resulting OL sfmc at 36-km resolution only increases after the day of the landslide occurrence and OL sfmc at 9-km resolution keeps decreasing.

The examples (Fig. 8) show that individual landslides are not necessarily happening for unique or well-defined values of land surface variables but rather different combinations thereof, for example, nearly saturated conditions (low catdef) coinciding with an additional, small rainfall event. Additionally, the simulations have limitations and might not accurately capture the conditions at the landslides' slopes.

2) PROBABILITY DENSITY DISTRIBUTIONS

More general insight into which land surface conditions are typically associated with landslide events can be obtained

by creating probability density functions of the simulated land surface variables for the LSE and noLSE subsets. Figure 9 and Table 2 summarize the LSE and noLSE distribution characteristics for OL sfmc, rzmc, prmc, catdef (only for the SMOS-GRACE study period), rainfall and ARI7, with 4131 (2747) LSE samples, and about 4.2 million (2.1 million) noLSE samples for the SMOS-GRACE (SMAP) study period.

Overall, the results are similar for the SMOS-GRACE and SMAP study periods, as can be seen by comparing the top and bottom portions of Fig. 9, despite the differences in spatial resolutions and meteorological forcing data: the median and maximum of rainfall and ARI7 are much higher for the LSE subset (right side boxplot) than for the noLSE one (left side boxplot). The same is true for sfmc, rzmc, prmc, and the (inverted) catdef, although the difference in medians is less pronounced than for rainfall. For both study periods, the shape of the distributions of soil water content and rainfall is also very different between the LSE and noLSE subsets. The rainfall distributions are strongly exponential, both for the noLSE and LSE subset, but with a stronger peak at low to no rainfall for noLSE. For the ARI7, distributions change from strongly exponential for noLSE (similar to rainfall) to quasi-linear for LSE. Parameter A_{QQ} is largest for rainfall and ARI7, indicating that the difference between noLSE and LSE distributions is strongest for these variables (Table 2). The soil moisture distributions change shape from quasi-normal for noLSE (especially for rzmc and prmc) to more skewed or exponential distributions for LSE. The A_{QQ} decreases when a deeper soil column is considered ($A_{QQ, \text{sfmc}} > A_{QQ, \text{rzmc}} > A_{QQ, \text{prmc}}$) with the exception of catdef ($A_{QQ, \text{catdef}} > A_{QQ, \text{sfmc}}$), indicating that catdef indeed holds information beyond what can be provided by sfmc to discern between stable and sliding slopes (Table 2). Table 2 further also shows the differences in skewness and kurtosis of the described distributions.

Figure 10 demonstrates that when transforming a land surface variable (here rzmc), the shapes of the noLSE and LSE distributions are profoundly changed, and, in contrast to the original data without transformation, the landslide probability [being proportional to the conditional distribution $p(\text{rzmc}|\text{LSE})$] steadily increases with increasing percentile values. Table 3 shows that, after percentile transformations, the distribution metrics become more similar across the various land surface variables and differences between noLSE and LSE

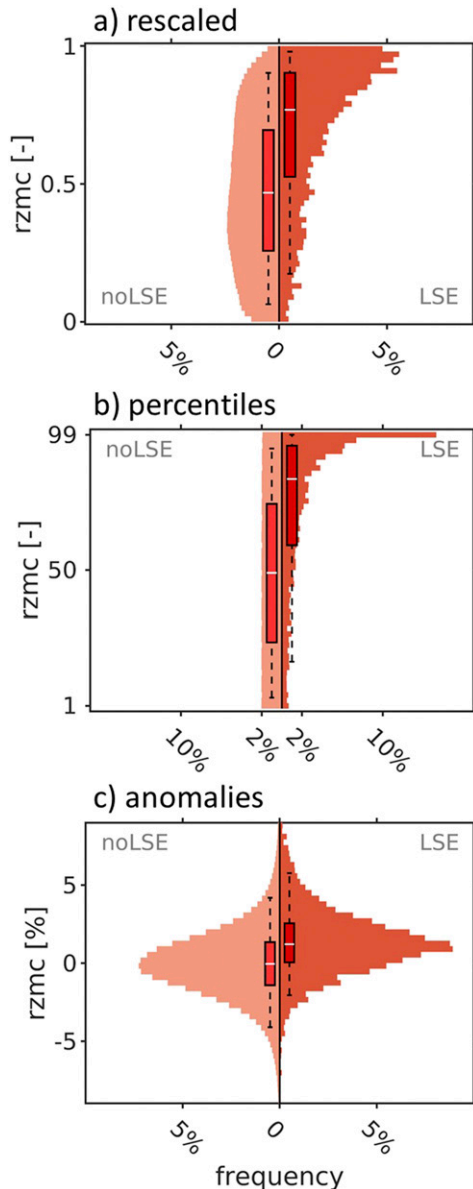


FIG. 10. Distribution of model-only (OL) rzmc for the SMOS-GRACE study period. (right, dark color) LSE and (left, light color) noLSE are shown in (background) histograms and (foreground) boxplots and for different transformations: (a) linearly rescaled, (b) as percentiles, or (c) as anomalies. For distributions without transformation (volumetric rzmc), see Fig. 9.

distributions are larger, i.e., the A_{QQ} values are larger and the shift in skewness and kurtosis from noLSE to LSE is larger. This finding is similar (not shown) for linearly rescaled data.

Of the soil water content variables, sfmc and catdef exhibit the largest differences between noLSE and LSE distributions without transformation, and sfmc is most different between noLSE and LSE after transformation (Tables 2 and 3). This is largely driven by short-term rainfall extremes, i.e., the shallower sfmc is more closely connected to rainfall and ARI7.

Since we want to add extra information beyond what can be extracted from merely rainfall-driven sfmc, in the following we focus on rzmc as the explaining variable for landslide probabilities in line with previous studies (section 1), and because rzmc incorporates information from both sfmc and catdef.

d. Impact of data assimilation at landslide events

We now turn toward the question if merging model and satellite data via DA would be beneficial for landslide modeling. The time series examples for the landslides in Canada and Colombia (Fig. 8) also illustrate how the different satellite observations influence the various DA estimates of soil moisture (sfmc, rzmc) and water table depth (catdef). For both locations, the available SMOS soil moisture retrievals do not fulfill the highest quality standards (SMOS-SM1 not available) and only some SMOS-Tb are available, so that DA_SMOS-SM1 and DA_SMOS-Tb only deviate slightly from the OL simulation. The SMOS retrievals do fulfill minimum quality standards, which introduce short-term DA_SMOS-SM0 updates in sfmc and longer lasting updates in rzmc, especially for the landslide in Colombia. DA_GRACE updates the modeled catdef and thereby indirectly influences sfmc and rzmc. When assimilating both SMOS-SM0 and GRACE TWS (DA_SMOS-GRACE), the resulting sfmc, rzmc and catdef are in between the single-sensor DA_SMOS-SM0 and DA_GRACE. For DA_SMAP-Tb, the water content variables remain nearly unaltered for the landslide in Canada despite the availability of suitable observations, whereas the water content is slightly increased for the landslide in Colombia.

To measure the impact of DA, we count how often, on days of landslide occurrence, DA rzmc is higher or lower than OL rzmc, i.e., counting $n_{\Delta rzmc,+}$ and $n_{\Delta rzmc,-}$ only for the LSE subset [see Eq. (4) and section 2c(4)]. Figure 11a summarizes these counts for all landslide events, presented as percentages relative to the total number of landslides (i.e., 4131 during the SMOS-GRACE study period and 2747 during the SMAP study period). DA_GRACE, DA_SMOS-SM0 and DA_SMOS-GRACE result in $n_{\Delta rzmc,-} > n_{\Delta rzmc,+}$ (negative net impact). For about half the landslide events (and more for DA_SMOS-SM1, DA_SMOS-Tb and DA_SMAP-Tb), $\Delta rzmc$ is less than a minimum threshold of 2% of the local maximum rzmc. Only for DA_SMAP-Tb, there is a tendency toward wetter rzmc at landslide events after assimilation, i.e., $n_{\Delta rzmc,+} > n_{\Delta rzmc,-}$ (positive net impact). Still, the rzmc remains virtually unchanged for more than 75% of the landslide events during this study period.

However, as discussed in section 2c(1), in terms of raw volumetric values of rzmc, the assumption of a higher landslide probability with increased rzmc does not fully hold, whereas the assumption can be upheld after transforming rzmc via linear rescaling or into percentiles. For rescaled rzmc (Fig. 11b), the net impacts remain similar to those for the raw rzmc, but with larger $n_{\Delta rzmc,+}$ and $n_{\Delta rzmc,-}$. Through the stretching process (see Fig. 10a), $\Delta rzmc$ now crosses the 2% minimum threshold more often. Percentiles of rzmc (see Figs. 10b and 11c) exhibit a larger $n_{\Delta rzmc,+}$ and a smaller $n_{\Delta rzmc,-}$, with again the most positive net impact for DA_SMAP-Tb, i.e., the probability for a landslide at

TABLE 3. As in Table 2, but for percentile values.

	36-km OL (SMOS-GRACE study period)					9-km OL (SMAP study period)				
	A_{QQ}	Skewness		Kurtosis		A_{QQ}	Skewness		Kurtosis	
		LSE	noLSE	LSE	noLSE		LSE	noLSE	LSE	noLSE
Rainfall	0.60	−1.50	0.02	4.65	1.81	0.52	−1.32	0.08	3.94	1.82
ARI7	0.62	−1.49	0.01	4.92	1.81	0.63	−1.56	0.01	4.93	1.80
sfmc	0.58	−1.33	0.01	3.96	1.80	0.64	−1.53	0.01	4.81	1.80
rzmc	0.50	−1.08	0.01	3.17	1.80	0.56	−1.24	0.01	3.73	1.80
prmc	0.47	−1.01	0.01	2.97	1.80	0.53	−1.15	0.01	3.47	1.80
catdef	0.44	−0.91	0.01	2.75	1.80	—	—	—	—	—

the updated water content slightly increases. In terms of rzmc anomalies, which involves a nonlinear transformation for which the assumed monotonous increase of landslide probability with increased rzmc again does not hold (see Fig. 10c), no net impact of the various DA systems was found (Fig. 11d).

Regardless of the transformation, only some impact can be detected for about 50% of the landslides for DA_GRACE or DA_SMOS-GRACE, and for a much lower percentage in the other experiments, simply because not enough suitable microwave-based observations were assimilated at or near the considered landslides. When only taking into account grid boxes where at least one satellite observation is available during the study period (Figs. 11e–h), the results remain ambiguous for the various 36-km DA experiments in the SMOS-GRACE study period, whereas the 9-km DA_SMAP-Tb keeps showing a positive impact. Note that here the reference number of total landslide events changes (numbers at bottom), which explains the higher percentages especially for DA_SMOS-SM1 and DA_SMOS-Tb.

The net positive impact of DA is considerably more prevalent when only considering landslides for which the OL rzmc was <50th percentile (Figs. 11i–l). The key result is in Fig. 11k: the rzmc percentiles are predominantly increased for all DA experiments. Even though the OL rzmc is <50th percentile for only a small fraction of all landslides, this result is crucial, as it reveals a spatially and temporally localized benefit of soil moisture DA, where OL rzmc and rainfall alone would miss a potential landslide risk. This result is also a warning that DA has limitations at the edges of the soil moisture range: for situations where OL rzmc is already close to complete soil saturation, there might be no room for an increase in rzmc through DA and the chance of decreasing rzmc via satellite DA is much higher. Similarly, chances of increasing rzmc through DA at lower values are generally higher as well.

Spatial distributions of the net impact of DA_SMOS-GRACE and DA_SMAP-Tb per grid box with landslide events are presented in Fig. 12 for the percentile transformation (i.e., Fig. 11c). The distribution of positive or negative net impacts confirms that no obvious geographic factor can explain where the assimilation helps to increase the probability of a landslide (by increasing the soil water content) at landslides and where not.

To summarize, DA_SMAP-Tb (i.e., the SMAP L4 product) at 9-km resolution is overall beneficial for landslide probability modeling. However, the SMAP L4 and OL estimates are similar for a large fraction of landslides where SMAP T_b

observations cannot easily be converted to soil moisture. Assimilating SMOS and GRACE at 36-km resolution is beneficial only when the OL rzmc is not wet already, and with more impact when more observations are assimilated, or when larger soil volumes are updated by including GRACE DA.

4. Discussion

In line with previous smaller scale studies on modeled soil water content (e.g., Ponziani et al. 2012; Segoni et al. 2018), our global-scale study confirms that, despite unavoidable errors in both the landslide information and model simulations, clear differences in sampled $p(x_i|\text{LSE})$ and $p(x_i|\text{noLSE})$ are found for a range of CLSM OL land surface variables x_i . The fact that differences between stable and landslide conditions are not as strong for OL soil moisture and water table depth as for rainfall and ARI7 is a result of the nature of these very different variables. When transforming the data into percentiles, the landslide probabilities monotonously and similarly increase with soil water contents and rainfall. Further work is needed to investigate whether these climatological differences are sufficient to actually discern between stable and landslide-favoring conditions in a probabilistic way, and whether our approach can be extended to shorter time scales, e.g., to distinguish between stable and landslide conditions within a storm period.

Our results indicate that merging CLSM with SMOS and GRACE satellite observations via DA does no particular harm or good across all landslides. In part, this is due to the mentioned gaps in SMOS observations. The horizontal propagation of information via spatial filtering is also not powerful enough to accurately update soil moisture in complex areas. The GRACE DA has a greater impact on soil water estimates, because of the greater availability of GRACE observations and the update of water amounts in a larger soil volume. Furthermore, most landslides occur at high soil water content, reducing the chances for DA to further increase moisture content values.

An obscuring factor of the 36-km experiments is that the uncorrected MERRA-2 rainfall forcing may temporally overestimate rainfall in the tropics (Gelaro et al. 2017; Reichle et al. 2017a). If this bias were only seasonal and not fully removed from the assimilation system (which corrects for climatological bias), then the coarse-scale satellite data would likely attempt to correct saturated simulations toward lower soil moisture,

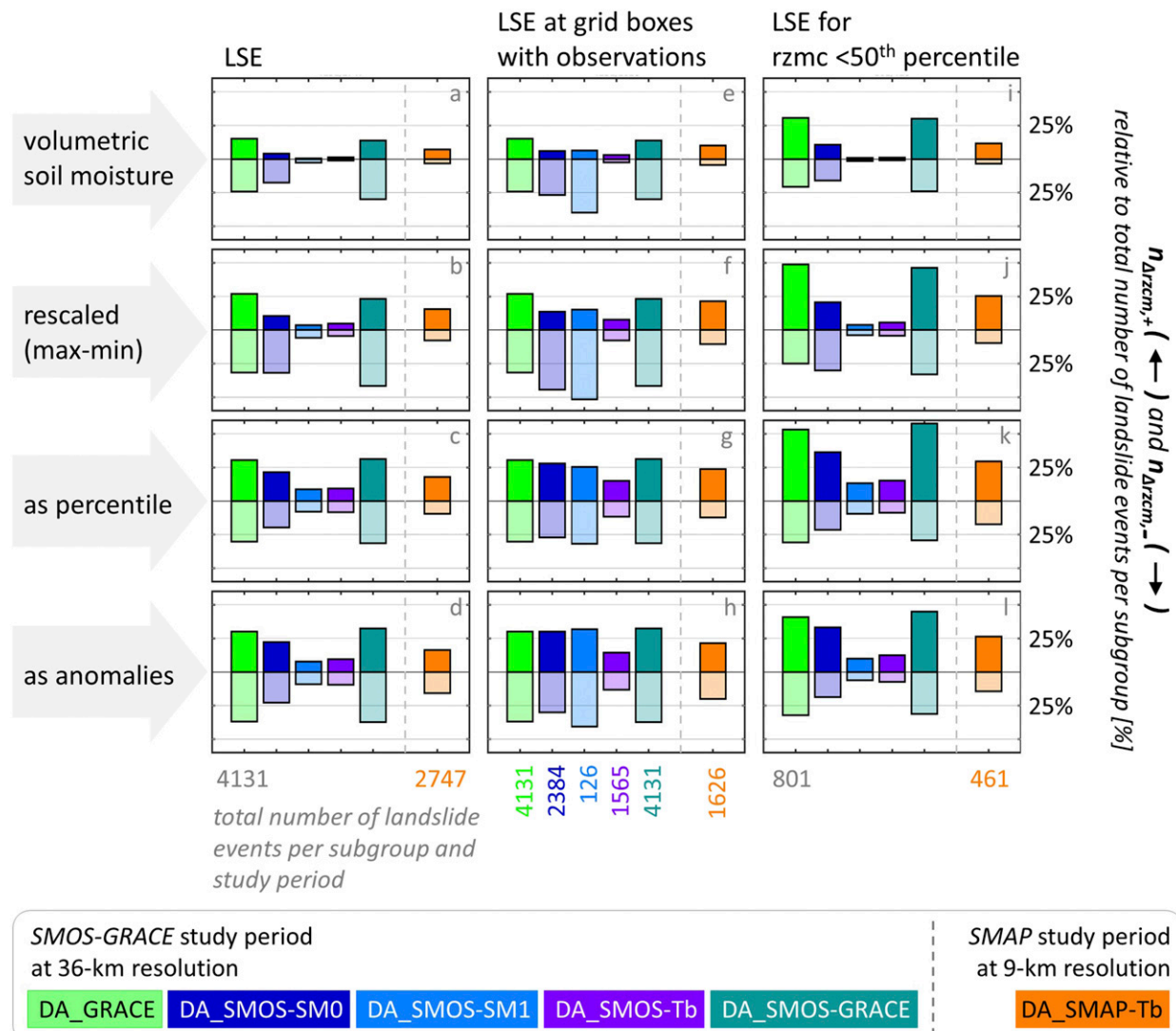


FIG. 11. Effect of DA and data transformation on rzmc conditioned on LSE: number of instances for positive (dark color, $n_{\Delta rzmc,+}$) and negative (light color, $n_{\Delta rzmc,-}$) $\Delta rzmc$ for different assimilation systems at 36- and 9-km resolution. (a)–(d) Counts for all landslide occurrences during the study period, (e)–(h) only taking grid boxes with observations into account, (i)–(l) for landslides on days with OL rzmc < 50th percentile. The $\Delta rzmc$ with absolute values below a minimum threshold of 2% of the maximum OL rzmc within a grid box are excluded. For values transformed to percentiles the threshold is intrinsically the percentile interval size. The total number of landslides per subgroup and study period are indicated at the bottom.

because the coarse satellite footprint covers a heterogeneous scene that rarely experiences complete soil saturation. In any case, a stratification of the 36-km results based on OL rzmc reveals that DA indeed has a beneficial effect and increases the soil water content at observed landslides, when the simulated OL rzmc is not very wet already, e.g., when the model missed a precipitation event.

The SMAP DA at 9-km resolution is generally more beneficial for landslide modeling, but one should keep in mind that the analysis was carried out for a different time period and set of landslide events. Although SMOS and SMAP observations are very similar (Burgin et al. 2017), the SMAP sensor is less prone to RFI contamination, possibly showing in the DA

performance at landslide events. Furthermore, the gauge-corrected precipitation and the higher spatial resolution of the SMAP L4 product, as well as more reliable landslide data from the GLC for the later study period could be adding to the beneficial effect. It is interesting that the inclusion of gauge-corrected precipitation already creates superior 9-km OL simulations for the SMAP study period in comparison to the SMOS-GRACE study period, but SMAP DA is still able to add value (Reichle et al. 2021), also for landslide modeling.

Of course, the process of dynamic land surface model simulation and DA is more computationally intensive than calculating a soil moisture proxy, such as the ARI7 (Kirschbaum and Stanley 2018).

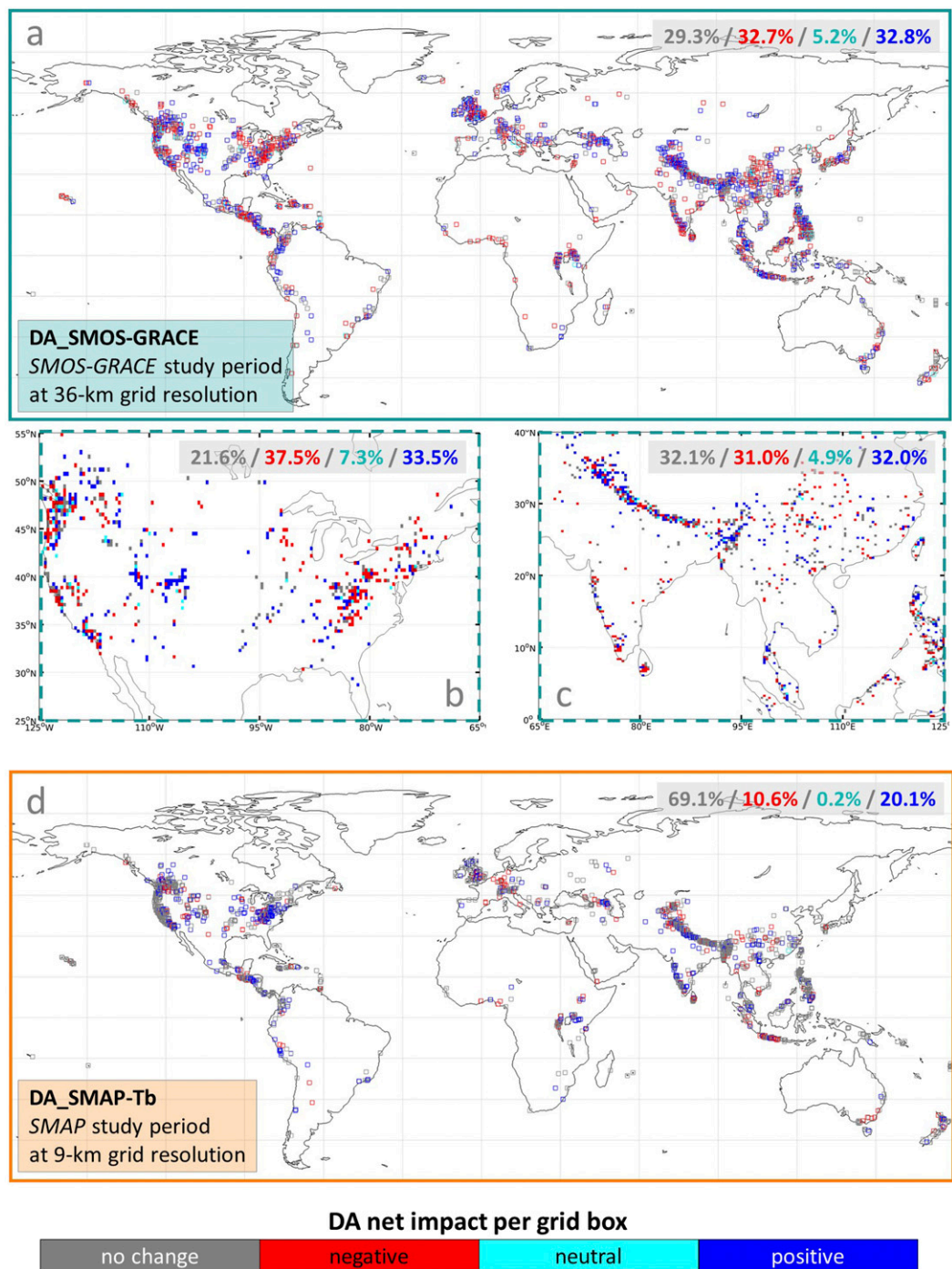


FIG. 12. Spatial distribution of the DA net impact per grid box for rzmc percentiles, conditioned on LSE. (a)–(c) DA_SMOS-GRACE at 36-km resolution: (a) global, (b) for North America, (c) for Southeast Asia. (d) DA_SMAP-Tb at 9-km resolution. Colors are as follows: positive net impact: $n_{\Delta rzmc,+} > n_{\Delta rzmc,-}$ (blue); neutral net impact: $n_{\Delta rzmc,+} = n_{\Delta rzmc,-}$ (cyan); negative net impact: $n_{\Delta rzmc,+} < n_{\Delta rzmc,-}$ (red); rzmc at LSE remains unchanged by DA (gray). Percentages of no change, negative, neutral and positive changes per map are given in the upper-right corners.

However, land surface model and DA results enable a physically based integration and downscaling of rainfall information within land surface model simulations at higher spatial resolutions, detaching landslide modeling resolutions from those

of available rainfall products. The SMAP L4 product is moreover readily available online with a latency of only 3 days (Reichle et al. 2019), which reduces the computational expense.

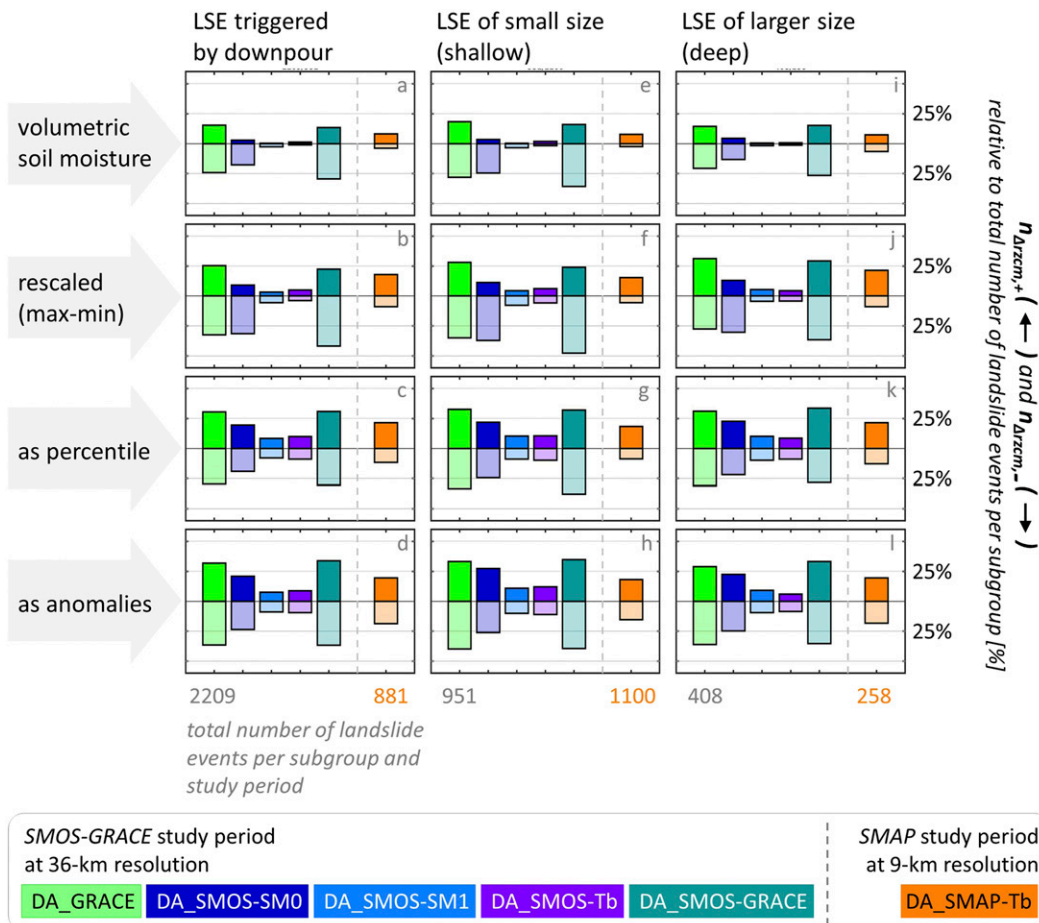


FIG. A1. As in Fig. 11, but for other subgroups: (a)–(d) only including landslides triggered by downpour (noted in the GLC), (e)–(h) only small (shallow) landslides, and (i)–(l) only large (deep-seated) landslides.

5. Conclusions

In this study we investigated whether global landslide modeling could benefit from soil water content and TWS estimates from remote sensing, a land surface model and data assimilation. An analysis of the probability density distributions for various soil water content and rainfall variables (and their transformations) at landslide events leads to the following conclusions:

- 1) Remotely sensed estimates of soil moisture (SMOS and SMAP) and TWS (GRACE) alone are not recommended for global landslide modeling. SMOS and SMAP data are intermittent in time and space and difficult to convert to moisture estimates in those complex terrain areas most susceptible to landslides. This results in observations only being available for less than 50% of landslide events during the study period (depending on quality standards). GRACE observations are available for about 75% of landslide events during the study period, but their very coarse spatial and temporal resolution is less suitable for landslide modeling as part of early warning systems.
- 2) Soil water estimates from a land surface model (CLSM) are able to statistically distinguish the land surface

- conditions for “stable slopes” (noLSE) and “landslides” (LSE). Advantages of CLSM simulations are the complete spatial and temporal coverage (with optional increases in resolution in space and time) and the information on soil water content at different depths. Rainfall and ARI7 exhibit the largest differences between noLSE and LSE distributions. However, when transforming model-only (OL) soil water content estimates to percentiles, the differences between noLSE and LSE distributions also become more pronounced for these variables and the landslide probability monotonously increases with soil water content percentiles. We advise relying on rzmc percentiles to distinguish between noLSE and LSE conditions, in order to include information on both rainfall and deeper water table variations.
- 3) Merging satellite data from SMOS and GRACE with land surface modeling (data assimilation, DA) is beneficial for landslide modeling when OL rzmc is <50th percentile. The SMAP L4 product is generally more beneficial, with consistently more rzmc increases than decreases at landslide events (LSE), regardless of the data transformation or the subset of considered landslides. However, DA can only add value over

OL output if the assimilated satellite observations can be meaningfully interpreted. For SMOS and SMAP, this is difficult near open water or in complex terrain. Furthermore, there are limitations to DA in near-saturated conditions.

To limit the risk of missing a landslide hazard, and based on the fact that estimates of soil water content were found to be reliable in earlier studies with similar assimilation systems (De Lannoy and Reichle 2016b; Giroto et al. 2016, 2019; Reichle et al. 2019), we suggest using DA products for landslide modeling when rainfall products alone or OL products suggest no risk, because this might simply be a result of underestimated precipitation and consequently underestimated OL soil water content. In the future, the potential of soil water content DA products to also limit false alarms needs to be investigated, and the use of higher-resolution data (e.g., from *Sentinel-1*), the advancement of inversion methods over complex terrains, as well as the integration of in situ soil moisture or groundwater table observations in landslide prone areas may further increase the benefit of DA.

Acknowledgments. We thank Elvira Vassilieva for her essential work of deducting information on landslide occurrences from reports in Russian language, and thank Luca Brocca and Matthias Vanmaercke for valuable contributions as part of the PhD supervisory committee of AF. The computational resources (High Performance Computing) and services used in this work were provided by the VSC (Flemish Supercomputer Center), funded by KU Leuven (C14/16/045), FWO (1512817N) and the Flemish Government. AF was funded by FWO-G0C8918N. R. Reichle was supported by the SMAP mission.

APPENDIX A

Additional Stratifications for Data Assimilation Impact Analysis

In an attempt to understand whether the net impact of DA on rzmc depends on the type of landslide or on particular environmental factors, the results are additionally stratified for the landslide trigger (at downpour, Figs. A1a–d), the landslide shear plane (shallow, Figs. A1e–h and deep seated, Figs. A1i–l) and regional, seasonal, and environmental characteristics (the latter are not shown). However, no stratification stands out. For 9-km DA_SMAP-Tb, the positive impact remains for most subgroups of landslides and transformations (with the exception of anomalies).

For lack of detailed information about the depths of the landslide's shear planes (d_{sp}) that would allow for a categorization into shallow (typically $d_{sp} < 3$ m) and deep landslides (typically $d_{sp} > 3$ m), we derived average depths from the GLC volume attributes for each landslide. Applying the relationship between landslide area A and volume V of Larsen et al. (2010), $V = 10^{-0.836} A^{1.332}$, we obtain a maximum depth of 0.42 m for landslides categorized as “small” in the GLC ($V < 10$ m³), and a minimum depth of 4.16 m for landslides categorized as “large,” “very large,” and “catastrophic” ($V > 1000$ m³). Based on our own evaluation using local data, these indicative depth estimates

based on the above formula are slightly underestimated, except when many small landslides are reported as an aggregated large landslide, which would result in an overestimated d_{sp} .

APPENDIX B

Abbreviations

ARI7	7-day antecedent rainfall index
catdef	Catchment deficit
CLSM	Catchment Land Surface Model
DA	Data assimilation
EASEv2	Equal-Area Scalable Earth version 2
EnKF	Ensemble Kalman filter
GEOS	Goddard Earth Observing System
GLC	Global Landslide Catalog
GRACE	Gravity Recovery and Climate Experiment
GSFC	Goddard Space Flight Center
LHASA	Landslide Hazard Assessment for Situational Awareness
LSE	Landslide event
MERRA-2	Modern-Era Retrospective Analysis for Research and Applications, version 2
noLSE	No landslide event
OL	Open loop, i.e., model-only
prmc	Profile soil moisture content
RFI	Radio frequency interference
rzexc	Root-zone excess
rzmc	Root-zone soil moisture content
sfmc	Surface soil moisture content
SMAP	Soil Moisture Active Passive
SMAP L4	SMAP Level-4 surface and root-zone soil moisture product
SMAP study period	Study period April 2015–December 2019
SMOS	Soil Moisture Ocean Salinity
SMOS-GRACE study period	Study period January 2011–July 2016
srfexc	Surface excess
T_b	Brightness temperature
TWS	Terrestrial water storage

REFERENCES

- Bechtold, M., and Coauthors, 2019: PEAT-CLSM: A specific treatment of peatland hydrology in the NASA catchment land surface model. *J. Adv. Model. Earth Syst.*, **11**, 2130–2162, <https://doi.org/10.1029/2018MS001574>.
- Bogaard, T., and R. Greco, 2018: Invited perspectives: Hydrological perspectives on precipitation intensity-duration thresholds for landslide initiation: Proposing hydro-meteorological thresholds. *Nat. Hazards Earth Syst. Sci.*, **18**, 31–39, <https://doi.org/10.5194/nhess-18-31-2018>.
- Brocca, L., F. Ponziani, T. Moramarco, F. Melone, N. Berni, and W. Wagner, 2012: Improving landslide forecasting using ASCAT-derived soil moisture data: A case study of the Torgiovannetto landslide in central Italy. *Remote Sens.*, **4**, 1232–1244, <https://doi.org/10.3390/rs4051232>.
- , L. Ciabatta, T. Moramarco, F. Ponziani, N. Berni, and W. Wagner, 2016: Use of satellite soil moisture products for

- the operational mitigation of landslides risk in Central Italy. *Satellite Soil Moisture Retrieval*, P. K. Srivastava, G. P. Petropoulos, and Y. H. Kerr, Eds., Elsevier, 231–247, <https://doi.org/10.1016/B978-0-12-803388-3.00012-7>.
- Burgin, M. S., and Coauthors, 2017: A comparative study of the SMAP passive soil moisture product with existing satellite-based soil moisture products. *IEEE Trans. Geosci. Remote Sens.*, **55**, 2959–2971, <https://doi.org/10.1109/TGRS.2017.2656859>.
- Caine, N., 1980: The rainfall intensity: Duration control of shallow landslides and debris flows. *Geogr. Ann.*, **62A**, 23–27, <https://doi.org/10.2307/520449>.
- Chen, F., W. T. Crow, R. Bindlish, A. Colliander, M. S. Burgin, J. Asanuma, and K. Aida, 2018: Global-scale evaluation of SMAP, SMOS and ASCAT soil moisture products using triple collocation. *Remote Sens. Environ.*, **214**, 1–13, <https://doi.org/10.1016/j.rse.2018.05.008>.
- Dai, A., 2006: Precipitation characteristics in eighteen coupled climate models. *J. Climate*, **19**, 4605–4630, <https://doi.org/10.1175/JCLI3884.1>.
- De Lannoy, G. J. M., and R. H. Reichle, 2016a: Global assimilation of multiangle and multipolarization SMOS brightness temperature observations into the GEOS-5 catchment land surface model for soil moisture estimation. *J. Hydrometeorol.*, **17**, 669–691, <https://doi.org/10.1175/JHM-D-15-0037.1>.
- , and —, 2016b: Assimilation of SMOS brightness temperatures or soil moisture retrievals into a land surface model. *Hydrol. Earth Syst. Sci.*, **20**, 4895–4911, <https://doi.org/10.5194/hess-20-4895-2016>.
- , R. D. Koster, R. H. Reichle, S. P. P. Mahanama, and Q. Liu, 2014: An updated treatment of soil texture and associated hydraulic properties in a global land modeling system. *J. Adv. Model. Earth Syst.*, **6**, 957–979, <https://doi.org/10.1002/2014MS000330>.
- Entekhabi, D., and Coauthors, 2010: The Soil Moisture Active Passive (SMAP) mission. *Proc. IEEE*, **98**, 704–716, <https://doi.org/10.1109/JPROC.2010.2043918>.
- Froude, M. J., and D. N. Petley, 2018: Global fatal landslide occurrence from 2004 to 2016. *Nat. Hazards Earth Syst. Sci.*, **18**, 2161–2181, <https://doi.org/10.5194/nhess-18-2161-2018>.
- FSBIH, 2018: Federal State Budgetary Institution “Hydrospektgeology”: Archive of quarter annual reports of exogenous geological processes on territories of the Russian Federation. Accessed 3 February 2021, <https://geomonitoring.ru/arxiv.html>.
- Gelaro, R., and Coauthors, 2017: The Modern-Era Retrospective Analysis for Research and Applications, version 2 (MERRA-2). *J. Climate*, **30**, 5419–5454, <https://doi.org/10.1175/JCLI-D-16-0758.1>.
- Giroto, M., G. J. M. De Lannoy, R. H. Reichle, and M. Rodell, 2016: Assimilation of gridded terrestrial water storage observations from GRACE into a land surface model. *Water Resour. Res.*, **52**, 4164–4183, <https://doi.org/10.1002/2015WR018417>.
- , R. H. Reichle, M. Rodell, Q. Liu, S. Mahanama, and G. J. M. De Lannoy, 2019: Multi-sensor assimilation of SMOS brightness temperature and GRACE terrestrial water storage observations for soil moisture and shallow groundwater estimation. *Remote Sens. Environ.*, **227**, 12–27, <https://doi.org/10.1016/j.rse.2019.04.001>.
- Glade, T., M. Crozier, and P. Smith, 2000: Applying probability determination to refine landslide-triggering rainfall thresholds using an empirical “Antecedent daily rainfall model.” *Pure Appl. Geophys.*, **157**, 1059–1079, <https://doi.org/10.1007/s000240050017>.
- Guzzetti, F., S. Peruccacci, M. Rossi, and C. P. Stark, 2007: Rainfall thresholds for the initiation of landslides in central and Southern Europe. *Meteor. Atmos. Phys.*, **98**, 239–267, <https://doi.org/10.1007/s00703-007-0262-7>.
- Hong, Y., R. Adler, and G. Huffman, 2006: Evaluation of the potential of NASA multi-satellite precipitation analysis in global landslide hazard assessment. *Geophys. Res. Lett.*, **33**, L22402, <https://doi.org/10.1029/2006GL028010>.
- Kerr, Y. H., and Coauthors, 2012: The SMOS soil moisture retrieval algorithm. *IEEE Trans. Geosci. Remote Sens.*, **50**, 1384–1403, <https://doi.org/10.1109/TGRS.2012.2184548>.
- Kidd, C., A. Becker, G. J. Huffman, C. L. Muller, P. Joe, G. Skofronick-Jackson, and D. B. Kirschbaum, 2017: So, how much of the Earth’s surface is covered by rain gauges? *Bull. Amer. Meteor. Soc.*, **98**, 69–78, <https://doi.org/10.1175/BAMS-D-14-00283.1>.
- Kirschbaum, D., and T. Stanley, 2018: Satellite-based assessment of rainfall-triggered landslide hazard for situational awareness. *Earth’s Future*, **2018**, 505–523, <https://doi.org/10.1002/2017EF000715>.
- , R. Adler, Y. Hong, S. Hill, and A. Lerner-Lam, 2010: A global landslide catalog for hazard applications: Method, results, and limitations. *Nat. Hazards*, **52**, 561–575, <https://doi.org/10.1007/s11069-009-9401-4>.
- , T. Stanley, and Y. Zhou, 2015: Spatial and temporal analysis of a global landslide catalog. *Geomorphology*, **249**, 4–15, <https://doi.org/10.1016/j.geomorph.2015.03.016>.
- , —, R. Emberson, P. Amatya, S. Khan, and H. Tanyas, 2020: Global Landslide Hazard Assessment for Situational Awareness (LHASA) version 2: New activities and future plans. *EGU General Assembly 2020*, Online, European Geophysical Union, EGU2020-11012, <https://doi.org/10.5194/egusphere-egu2020-11012>.
- Koster, R. D., M. J. Suarez, A. Ducharme, M. Stieglitz, and P. Kumar, 2000: A catchment-based approach to modeling land surface processes in a general circulation model: 1. Model structure. *J. Geophys. Res.*, **105**, 24 809–24 822, <https://doi.org/10.1029/2000JD900327>.
- , S. D. Schubert, H. Wang, S. P. Mahanama, and A. M. DeAngelis, 2019: Flash drought as captured by reanalysis data: Disentangling the contributions of precipitation deficit and excess evapotranspiration. *J. Hydrometeorol.*, **20**, 1241–1258, <https://doi.org/10.1175/JHM-D-18-0242.1>.
- Larsen, I. J., D. R. Montgomery, and O. Korup, 2010: Landslide erosion controlled by hillslope material. *Nat. Geosci.*, **3**, 247–251, <https://doi.org/10.1038/ngeo776>.
- Leonarduzzi, E., P. Molnar, and B. W. McArdell, 2017: Predictive performance of rainfall thresholds for shallow landslides in Switzerland from gridded daily data. *Water Resour. Res.*, **53**, 6612–6625, <https://doi.org/10.1002/2017WR021044>.
- Loomis, B. D., S. B. Luthcke, and T. J. Sabaka, 2019: Regularization and error characterization of GRACE mascons. *J. Geod.*, **93**, 1381–1398, <https://doi.org/10.1007/s00190-019-01252-y>.
- Luthcke, S. B., T. J. Sabaka, B. D. Loomis, A. A. Arendt, J. J. McCarthy, and J. Camp, 2013: Antarctica, Greenland and Gulf of Alaska land-ice evolution from an iterated GRACE global mascon solution. *J. Glaciol.*, **59**, 613–631, <https://doi.org/10.3189/2013JoG12J147>.
- Mirus, B. B., M. D. Morpheus, and J. B. Smith, 2018: Developing hydro-meteorological thresholds for shallow landslide initiation and early warning. *Water*, **10**, 1274, <https://doi.org/10.3390/w10091274>.
- , D. M. Staley, J. W. Kean, J. B. Smith, R. Wooten, L. A. McGuire, and B. A. Ebel, 2019: Conceptual framework for assessing disturbance impacts on debris-flow initiation thresholds across hydroclimatic settings. *Proc. Seventh Int. Conf. on*

- Debris-Flow Hazards Mitigation*, Golden, CO, Association of Environmental Engineering Geologists, 8 pp., <https://doi.org/10.25676/11124/173176>.
- Monsieurs, E., O. Dewitte, and A. Demoulin, 2019: A susceptibility-based rainfall threshold approach for landslide occurrence. *Nat. Hazards Earth Syst. Sci.*, **19**, 775–789, <https://doi.org/10.5194/NHESS-19-775-2019>.
- Peltier, W. R., D. F. Argus, and R. Drummond, 2015: Space geodesy constrains ice age terminal deglaciation: The global ICE-6G_c (VM5a) model. *J. Geophys. Res. Solid Earth*, **120**, 450–487, <https://doi.org/10.1002/2014JB011176>.
- Petley, D., 2012: Global patterns of loss of life from landslides. *Geology*, **40**, 927–930, <https://doi.org/10.1130/G33217.1>.
- Piepmeyer, J. R., and Coauthors, 2017: SMAP L-band microwave radiometer: Instrument design and first year on orbit. *IEEE Trans. Geosci. Remote Sens.*, **55**, 1954–1966, <https://doi.org/10.1109/TGRS.2016.2631978>.
- Ponziani, F., C. Pandolfo, M. Stelluti, N. Berni, L. Brocca, and T. Moramarco, 2012: Assessment of rainfall thresholds and soil moisture modeling for operational hydrogeological risk prevention in the Umbria region (central Italy). *Landslides*, **9**, 229–237, <https://doi.org/10.1007/s10346-011-0287-3>.
- Qiu, J., J. Dong, W. T. Crow, X. Zhang, R. H. Reichle, and G. J. M. De Lannoy, 2021: The benefit of brightness temperature assimilation for the SMAP Level-4 surface and root-zone soil moisture analysis. *Hydrol. Earth Syst. Sci.*, **25**, 1569–1586, <https://doi.org/10.5194/hess-25-1569-2021>.
- Reichenbach, P., M. Rossi, B. D. Malamud, M. Mihir, and F. Guzzetti, 2018: A review of statistically-based landslide susceptibility models. *Earth-Sci. Rev.*, **180**, 60–91, <https://doi.org/10.1016/j.earscirev.2018.03.001>.
- Reichle, R. H., 2018: SMAP L4 global 3-hourly 9 km ease-grid surface and root zone soil moisture geophysical data, version 4. NASA National Snow and Ice Data Center DAAC, accessed 28 April 2020, <https://doi.org/10.5067/KPJNN2G11DQR>.
- , Q. Liu, R. D. Koster, C. S. Draper, S. P. P. Mahanama, and G. S. Partyka, 2017a: Land surface precipitation in MERRA-2. *J. Climate*, **30**, 1643–1664, <https://doi.org/10.1175/JCLI-D-16-0570.1>.
- , and Coauthors, 2017b: Assessment of the SMAP level-4 surface and root-zone soil moisture product using in situ measurements. *J. Hydrometeorol.*, **18**, 2621–2645, <https://doi.org/10.1175/JHM-D-17-0063.1>.
- , and Coauthors, 2019: Version 4 of the SMAP level-4 soil moisture algorithm and data product. *J. Adv. Model. Earth Syst.*, **11**, 3106–3130, <https://doi.org/10.1029/2019MS001729>.
- , Q. Liu, J. V. Ardizzone, W. T. Crow, G. J. M. De Lannoy, J. Dong, J. S. Kimball, and R. D. Koster, 2021: The contributions of gauge-based precipitation and SMAP brightness temperature observations to the skill of the SMAP level-4 soil moisture product. *J. Hydrometeorol.*, **22**, 405–424, <https://doi.org/10.1175/JHM-D-20-0217.1>.
- Rossi, M., S. Luciani, D. Valigi, D. Kirschbaum, M. T. Brunetti, S. Peruccacci, and F. Guzzetti, 2017: Statistical approaches for the definition of landslide rainfall thresholds and their uncertainty using rain gauge and satellite data. *Geomorphology*, **285**, 16–27, <https://doi.org/10.1016/j.geomorph.2017.02.001>.
- Segoni, S., A. Rosi, D. Lagomarsino, R. Fanti, and N. Casagli, 2018: Brief communication: Using averaged soil moisture estimates to improve the performances of a regional-scale landslide early warning system. *Nat. Hazards Earth Syst. Sci.*, **18**, 807–812, <https://doi.org/10.5194/nhess-18-807-2018>.
- Stanley, T. A., D. B. Kirschbaum, S. Sobieszczek, M. Jasinski, J. Borak, and S. Slaughter, 2020: Building a landslide hazard indicator with machine learning and land surface models. *Environ. Modell. Software*, **129**, 104692, <https://doi.org/10.1016/j.envsoft.2020.104692>.
- Swenson, S., J. Wahr, and P. C. D. Milly, 2003: Estimated accuracies of regional water storage variations inferred from the Gravity Recovery and Climate Experiment (GRACE). *Water Resour. Res.*, **39**, 1223, <https://doi.org/10.1029/2002WR001808>.
- Thomas, M. A., B. D. Collins, and B. B. Mirus, 2019: Assessing the feasibility of satellite-based thresholds for hydrologically driven landsliding. *Water Resour. Res.*, **55**, 9006–9023, <https://doi.org/10.1029/2019WR025577>.
- Whiteley, J. S., J. E. Chambers, S. Uhlemann, P. B. Wilkinson, and J. M. Kendall, 2019: Geophysical monitoring of moisture-induced landslides: A review. *Rev. Geophys.*, **57**, 106–145, <https://doi.org/10.1029/2018RG000603>.
- Wicki, A., P. Lehmann, C. Hauck, S. I. Seneviratne, P. Waldner, and M. Stähli, 2020: Assessing the potential of soil moisture measurements for regional landslide early warning. *Landslides*, **17**, 1881–1896, <https://doi.org/10.1007/s10346-020-01400-y>.
- Zaitchik, B. F., M. Rodell, and R. H. Reichle, 2008: Assimilation of GRACE terrestrial water storage data into a land surface model: Results for the Mississippi river basin. *J. Hydrometeorol.*, **9**, 535–548, <https://doi.org/10.1175/2007JHM951.1>.
- Zhuo, L., Q. Dai, D. Han, N. Chen, B. Zhao, and M. Berti, 2019: Evaluation of remotely sensed soil moisture for landslide hazard assessment. *IEEE J. Sel. Top. Appl. Earth Obs. Remote Sens.*, **12**, 162–173, <https://doi.org/10.1109/JSTARS.2018.2883361>.